1
High-Speed Microfluidic Manipulation of Cells

Aram J. Chung and Soojung Claire Hur

1.1
Introduction

The ability to manipulate biological cells is extremely useful for various biomedical and industrial applications. The grand challenge is determining how to manipulate cells (i) precisely (i.e., in a controlled manner), (ii) noninvasively (i.e., mimicking biological environment), and (iii) rapidly (i.e., high processing rate). In order to realize ideal cell manipulation, a microfluidics-based technique has been employed and explored extensively as a prime approach [1, 2]. This is largely because microfluidics-based cell manipulations provide unique opportunities for sophisticated and advanced biological assays. For example, an intrinsic laminar flow phenomenon allows for localized subcellular spatial and temporal flow control [3, 4]. In addition, the possibility of handling large numbers of cells via massive parallelization enables high-throughput single-cell processes [5–7], and the potential integration with other modalities permits fully integrated and automated systems [8, 9].

In this chapter, we will mainly discuss recent advancements in microfluidic cell manipulation techniques, which operate in a "high-speed" manner. General cell manipulation techniques using microchannels have been thoroughly reviewed and can be found elsewhere [10–15]. A high-speed process is extremely crucial for cell manipulation because the process speed directly correlates with biological sample volumes (i.e., throughput) that the technique is capable of analyzing. In fact, the demand is increasing for cell manipulation techniques that can process large volumes of biofluids (on the order from milliliters to liters), such as blood, pleural fluid, and urine [16–18]. High-speed cell manipulation is especially required to minimize residence times of cellular samples in microfluidic devices when off-chip analyses are necessary. Furthermore, there still remain many challenges to resolve cytotoxicity associated with extended cell residence times in microfluidic platforms [19].

Micro- and Nanomanipulation Tools, First Edition. Edited by Yu Sun and Xinyu Liu.

We will interchangeably use cell processing rate (e.g., cells min^{-1}) and volumetric flow rate (e.g., $\mu l\, min^{-1}$) when we describe "high-speed" microfluidic cell manipulation techniques. The threshold values for "high speed" will vary with cellular manipulation purposes. This is a proper way to conduct meaningful comparisons among various techniques because analysis methods are contingent upon their biological research questions. For example, throughputs of individual cell interrogation and separation are incommensurable not only due to the types of biological samples, but also the desired measurements to be taken. It should be noted that the process time can be interpreted as time required for (i) sample preparations, (ii) processing a given volume, (iii) data analysis, and/or (iv) combinations of all mentioned. We mainly limit our discussion to the time that cells are residing in microfluidic devices, but we will discuss other time considerations as well. Finally, we exclude static cell manipulations from discussions, despite their massively parallel cell manipulation capabilities [5, 20], because of their predetermined and inflexible throughput.

As shown in Figure 1.1, cell manipulation in microfluidic devices can be categorized into *direct* (Section 1.2) and *indirect* (Section 1.3) methods. Individual cellular physical morphology can be modulated "directly" by applying forces, or cells' flowing path can be "indirectly" altered by external stimuli while the cell morphology remains intact within microfluidic platforms. First, we will introduce each cell manipulation technique, classify further based on its working principle, and discuss the advantages and disadvantages of the technology. We tabulated all techniques and summarized the cell processing rate based on the individual technique to easily compare all different approaches. In the last section, we briefly summarized the main ideas of this chapter and provided our outlook on microfluidics-based cell manipulation and insights on where the technology should head.

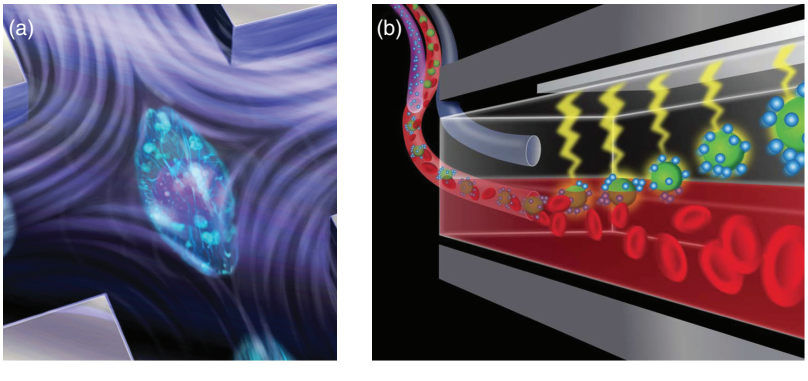

Figure 1.1 Two major examples of cell manipulation approaches in microfluidic channels, namely (a) direct cell [5] and (b) indirect cell manipulation [21].

1.2
Direct Cell Manipulation

Direct cellular manipulation involves processes that induce cell morphological changes under applied forces. The morphology of tested cells can be changed electrically, magnetically, optically, or mechanically [10–15]. We start by introducing each cell manipulation mechanism and discussing its advantages and limitations with respect to cell processing rate. Also, all direct cell manipulation techniques are tabulated in Table 1.1, comparing their characteristics.

1.2.1
Electrical Cell Manipulation

Electrical approaches, including patch clamp [22], impedance spectroscopy [23, 24], electroporation [25], and cell lysis [26], have been used to characterize and/or manipulate cells directly. Even though it is not possible to process a large number of cells rapidly due to challenging cell positioning tasks before cell manipulation, electrical cell manipulation techniques have elucidated many biologically meaningful cellular properties (e.g., size, membrane capacitance, and conductivity) and offered precise and relatively noninvasive cell manipulations [15].

One high-speed method from electrical techniques that should be highlighted is the impedance-based cell manipulation. The method monitors impedance changes in real time, allowing high-speed cellular property measurements. Typically, a current is generated by a conductive cell solution via metal electrodes with a small gap that are patterned on the substrate. The impedance changes are made when the cells pass over the electrodes (i.e., when the cells perturb the current path). For AC (alternating current) manipulation, most techniques are based on either low or intermediate frequencies. At low frequencies, the impedance amplitude indicates the cell size information since the cell membrane acts as a dielectric barrier, and at intermediate frequencies, membrane polarization is suppressed so that membrane properties can be obtained. Therefore, cell size, membrane, or cytoplasmic property information can be extracted based on impedance signatures [27, 28].

Because of its information richness, the technique was popularly used as an *impedance-based cytometer*. Reported sample processing rates based on impedance measurements can reach as high as 50 000 cells s^{-1} depending upon the operational electrical parameters and tested cellular characteristics [29]. Through this technology, distinct cellular properties from various cell types, including fibroblasts [30], leukocytes [31], adipocytes [30], cancer cell lines [32], and red blood cells (RBCs) [33, 34], were investigated. It should be noted that high-frequency-based impedance cytometers were also recently developed. At high frequencies, intracellular structures and cytosolic properties can be collected because of the negligibly polarized membranes [28]. Haandbæk *et al.* [35] reported an impedance cytometer discriminating wild-type yeast cells from

mutants at a high-frequency operating mode (up to 500 MHz) by characterizing subcellular components such as vacuoles. Since the calculated correlations are strongly influenced by cellular size and dielectric properties, often discrimination of cells with similar size/dielectric properties becomes a challenge. Despite this drawback, the impedance measuring technique is one of high-speed cell property measurement processes.

1.2.2 Magnetic Cell Manipulation

Magnetic cell manipulation approaches provide noninvasive, high-throughput, and efficient cell control [36, 37]. Conventional protocols to manipulate cells via magnetic forces require functionalizing cells with magnetic elements before cell interrogation; therefore, additional time should be considered for sample preparation. Most direct magnetic techniques, magnetic tweezers for example, operate under static flow conditions and are not in the scope of this chapter; however, detailed descriptions and their recent advances can be found elsewhere [38, 39]. Note that high-speed magnetic cell positioning and separation approaches as indirect cell manipulation methods are discussed separately in section "Magnetic Cell Separation".

1.2.3 Optical Cell Manipulation

An optical stretcher is a representative example of optical cell interrogation. Two laterally aligned optical fibers are used to create a spatially well-defined optical trap, stretching cells in microfluidic channels. As a powerful cell biophysical property measurement tool, optical cell stretchers have been mainly used for evaluating viscoelastic properties and deformability of various cell types such as RBCs, leukemia, and cancer cells [40–42]. This technique was applied as a cancer diagnostic tool as well [43]. As another prime optical cell manipulation method, optical tweezers have been used to manipulate cells for single-cell level biophysical studies [44, 45]. Optical tweezers utilize a tightly focused laser beam to trap cells by a momentum transfer, attracting cells into the center of the beam [46]. Optical tweezers are a versatile cell manipulation technique since the trapped cell can be manipulated directly by modulating the beam conditions and/or indirectly by translating the beam position. Even though optical cell manipulation techniques are not suited for performing high-throughput cell analysis ($N < 100$), it should be noted that their noninvasive nature allows for precise single-cell examination [47–49]. Extended use of the technique is anticipated if real-time data analysis capabilities and higher processing rates become possible [50].

1.2.4 Mechanical Cell Manipulation

In recent years, mechanical biomarkers (e.g., cell deformability) have gained much attention as an alternative to conventional molecular biomarkers (e.g., antibody conjugated with fluorescence) because measuring cell deformability simplifies complex detection schemes and can eliminate costly and lengthy cellular labeling and sample preparation processes [51, 52]. In order to induce cellular mechanical deformation, there are two major procedures that have been utilized in microfluidics, namely constriction-based (Section 1.2.4.1) and shear-induced (Section 1.2.4.2) cell manipulation.

1.2.4.1 Constriction-Based Cell Manipulation

Cell deformability is characterized by flowing cells through a narrow bottleneck region with a gap smaller than the cell diameter. Channels with a sudden narrowing or arrays of local constrictions (e.g., slits) are widely adopted designs (see Figure 1.2). In short, as suspended cells are injected into the microchannels, cells are forced to pass through a constriction(s), experiencing significant deformation. Depending on its purpose, constriction-based mechanical cell manipulation can be further classified into cell interrogation (see section "Constriction-Based Cell Interrogation") and cell separation (see section "Constriction-Based Cell Separation").

Constriction-Based Cell Interrogation

One of the major research focuses using constriction-based cell interrogation is investigating RBC biophysics, rheology, and associated diseases, including malaria, sickle cell disease, and sepsis [12, 52]. For instance, artesunate (ART) is a widely used drug for the treatment of malaria, and ART selectively induces stiffness changes in *Plasmodium falciparum*-infected RBCs, enabling identification of infected cells by monitoring cell transit velocity through a series of constrictions [59]. In addition, the deformability of RBCs from *Plasmodium yoelii*-infected mice was characterized to elucidate the correlation between splenic clearance and RBC deformability [60]. While great advancements were made understanding single-cell level biomechanical properties, most reported techniques operated at low processing rates ($1-2$ cells s^{-1}). Low-speed operation could be preferred for single-cell studies; however, higher processing rates should be addressed for cell state identification applications (i.e., diagnosis) to provide a statistical significance. Since constriction-based cell manipulation itself is often limited to high-speed cell processing, hybrid systems combining constriction-based cell deformation with other technologies, such as optics and electronics, were investigated. Another merit by integration with other modalities is multiparameter measurements, allowing precise cell characterizations. As shown in Figure 1.2a, Zheng *et al.* [53] reported a microfluidic platform combining electrical and mechanical modalities, obtaining signatures of each RBC, such as transit time, impedance amplitude ratio, and impedance phase increase with a

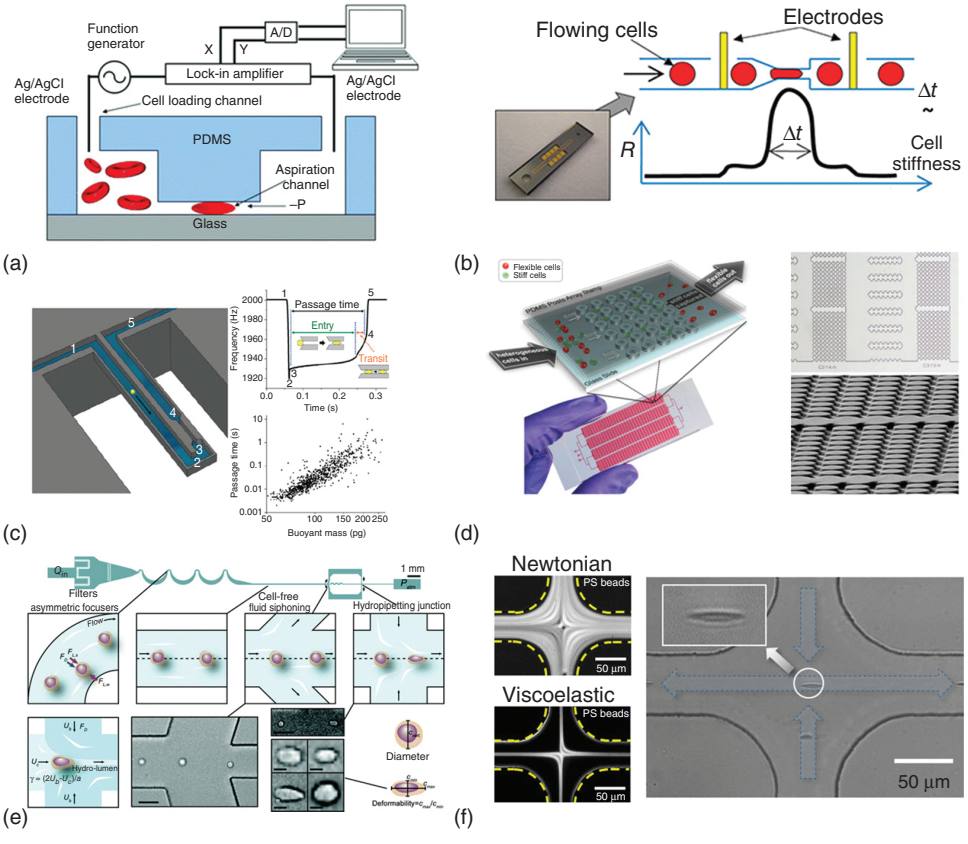

Figure 1.2 Direct cell manipulation techniques. Cell morphology can be manipulated (a,b) mechanically and electrically [53, 54], (c) mechanically and optically [55], (d) through cell and wall interactions [56], or (e,f) by pure hydrodynamic forces [57, 58].

throughput of 100–150 cells s^{-1}. Two Ag/AgCl electrodes were used to measure electrical impedance signals. By concentrating all electrical field lines to pass through the RBCs' membrane, higher cell responses were shown. In a similar manner, impedance measurements can be applied to cancer cells. Adamo *et al.* [54] reported a simple straight microchannel with a constriction where electrodes were patterned on the substrate (see Figure 1.2b). High-throughput (800 cells min^{-1}) HeLa cell interrogation was demonstrated and the correlations between transition time, cell stiffness, and size were reported. It should be noted that impedance-based platforms do not require a costly high-speed camera (more discussion can be found in Section 1.2.4.2), and real-time data acquisition is possible.

An optical approach was also combined with constriction-based cell deformation. A platform using a suspended microchannel resonator (SMR) was proposed (see Figure 1.2c) [55]. SMR consisted of a hollow microfluidic channel embedded in a silicon cantilever [61]. The resonance frequency is measured by the deflection

of a laser beam, and its changes were recorded as a cell enters the SMR and passes the local constriction. The frequency signatures were later translated into cell transit time and velocity information. Various cell types including mouse and human lung cancer cell lines, mouse embryonic fibroblasts, as well as a mouse lymphoblastic leukemia cell line were tested with high-speed processing rates of 10^5 and $\sim 10^3$ cells h^{-1}. While the SMR setup relies on highly complex, costly, and nontrivial fabrication and measurement techniques, higher throughput was shown and additional cell information (e.g., friction information) was able to be collected.

Constriction-Based Cell Separation

Cell separation was also demonstrated via channel geometry-induced cell deformation. Note that this section focuses on cell deformability-based sorting via channel constrictions, but general deformability-based cell separation is discussed in section "Deformability-Based Cell Separation" separately. Commonly, cells pass through an array of local constrictions whose gap dimension gradually decreases. Cell stiffness dictates the passage time, and separation is accomplished by the time difference. Zhang *et al.* [56] separated two distinct cell populations from a mixture of breast cancer cell lines (MDA-ME-436 and SUM 1479) using an array of microbarriers (see Figure 1.2d). Soft cells passed constrictions easily whereas stiff cells lagged or remained trapped so that resident time-dependent cell separation was attained with a throughput of 3.3×10^4 cells min^{-1} (2 ml h^{-1}). Similarly, Preira *et al.* [62] separated leukocytes from whole blood based on their stiffness using a flow rate as high as 100 ml h^{-1}, demonstrating a possibility for circulating tumor cell (CTC) detection.

The constriction-based mechanical cell manipulation technique (both interrogation and separation) provides label-free cellular property measurements and relatively simple cell processing procedures. However, there are a few fundamental drawbacks that should be mentioned from constriction-based cell manipulation techniques: (i) Cell–wall interaction: Interactions between the cell and channel wall play a critical role in affecting the cell passage phenomena. Each contribution from adhesion and friction should be decoupled and investigated separately, revealing pure deformability attributes. (ii) Clogging: Constriction-based platforms can hardly be free from clogging issues. Once the channel is clogged, a new chip must be used, and hence a robust operation for a long duration is hard to expect. One promising solution for clog-free cell filtration was recently reported [63] where the cross section of a microfluidic channel can be adjusted not only to de-clog but also to capture cells based on a combination of size and deformability with a throughput of 900 000 cells h^{-1}.

1.2.4.2 Shear-Induced Cell Manipulation

Cells can be directly manipulated with fluid flow as another mechanical cell manipulation method. Typically, a microchannel with a constriction whose cross-sectional dimension is larger than the cell diameter is used. Instead of cells that experience direct contact with channel walls, their shapes are modulated by flow

shear stress. This is an excellent approach to study cells because this phenomenon mimics biophysical environment. For example, when RBCs travel in blood capillaries, they experience significant shear stresses inducing deformation [64]. By monitoring dynamic cell shape changes under shear flow, RBC biophysics, such as deformation (e.g., elongation) [65], traveling motions/patterns [66], and adenosine triphosphate (ATP) release [67], were investigated. Despite its simple experimental approach, this method did not expand much because it suffers from at least one of the following drawbacks: (i) Nonuniform shear stress: Since cells were randomly distributed throughout the channel cross section, individual cells experience nonuniform shear stress. Cells traveling near the channel center or the wall experience different magnitudes of shear stresses, producing inconsistent data. (ii) Poor imaging: Without a proper cell positioning step, imaging becomes a great challenge because cells are traveling in all different imaging planes. (iii) Low throughput: Shear-induced cell manipulation techniques rely on relatively low flow speed and concentration for analysis, making the approach not ideal for high-speed cell processing.

For both constriction-based and shear-induced cell controls, cells should be transported by the flow to induce cell deformation; therefore, the flow rate simply determines the throughput of the system. In order to increase throughput, naively increasing the flow rate would seem like an easy solution; however, when the Reynolds number ($Re = \rho U L_c/\mu$: a dimensionless parameter describing the ratio of inertial and viscous forces, where ρ is the fluid density, U is the mean flow velocity, L_c is the characteristic length of the channel, and μ is the fluid viscosity) becomes nonzero, flow behavior significantly deviates from Stokes flow. For example, the cross-sectional profile of the hydrodynamic flow focusing distorts as Reynolds number increases [68, 69]. It is important to note that at finite Reynolds number ($Re \approx 10-100$), two inertial effects: *Inertial particle migration* and *secondary flows* can be found [70–72], and by taking advantage of these two effects, extremely high-speed cell manipulations are possible. The reader is directed to other reviews [70–72] to seek a complete background and underlying physics of inertial focusing.

Gossett *et al.* [73] demonstrated an inertial cell stretcher with a high-throughput cell processing rate (2000 cell s^{-1}). Cells were first inertially focused in the middle of the channel and hit the fluidic wall at the cross junction where extension flow stretches cells. The platform provides higher throughput, precise cell positioning, and higher strain rates. The device was used for identification of leukocytes and malignant pleural cells, and characterization of pluripotent stem cells. Later, Tse *et al.* [74] reported that the identical platform can be used as a clinical diagnostic tool. They created deformability maps by testing patient samples, which could potentially help reduce cytology-based laboratory workloads and assist clinical decision-making. As an alternative inertial cell stretching approach, recently Dudani *et al.* [57] reported a pinched-flow hydrodynamic stretcher (see Figure 1.2e). The platform utilizes a self-sheathing flow from a single input solution, and an order of magnitude higher throughput (65 000 cells s^{-1}) compared to the previous design [73, 74] was achieved.

Inertial cell stretchers [57, 73, 74] are based on two-position cell focusing with respect to a vertical axis [70–72]; thus, one of the imaging planes should be out of focus, resulting in blurry image collection. Considering cell flow velocity (as high as a few meters per second), blurriness of the recorded images is a critical issue. Focusing cells upstream in a single-stream (i.e., single focal plane) manner can be an effective solution (discussed in Section 1.3.2.1), although recently exploiting non-Newtonian fluids to focus cells in a microchannel was reported [58]. Cells flowing in non-Newtonian fluids experience an elastic force in addition to the inertial lift forces, migrating cells into the center of the channel [70]. Since all cells were positioned in the center of the channel [75, 76], the imaging quality was improved significantly and a uniform shear stress was applied. As shown in Figure 1.2f, RBCs were stretched in a cross junction [58], analogous to a hydrodynamic cell stretcher [73, 74] with a throughput of 110 cells s^{-1}. Non-Newtonian cell manipulation offers better imaging and uniform shearing, although lower strain rates and relatively slow processing rates compared to inertial focusing should be addressed in the future.

For inertia-based microfluidic platforms, the cell travels extremely fast; therefore, normally high-speed microscopy is employed to examine cell deformation events. High-speed microscopy records a large number of image stacks as a data-rich approach, revealing direct cell information; however, real-time processing remains a great challenge due to slow data transfer and computationally demanding image analysis. Moreover, a high-speed camera mounted to a microscope makes the system costly and limits potential for miniaturization. As a promising imaging solution, recently Goda *et al.* [77] reported an ultrafast optical imaging technology for automated, real-time, and high-throughput cell analysis [78]. The technique could be operated with a high cell processing rate (100 000 cells s^{-1}), but its requirement of a cell labeling process is a drawback. Therefore, more efforts to avoid high-speed microscopy or developments on faster image analysis strategies [79] should be made to further advance inertia-based cell manipulations (Table 1.1).

1.3 Indirect Cell Manipulation

This section discusses techniques that shift flowing paths of cells as indirect cell manipulation with a focus on high-speed processing. Cell path manipulation processes are normally conducted for two main objectives: cell separation (Section 1.3.1) and cell alignment (Section 1.3.2).

1.3.1 Cell Separation

We set two thresholds defining high-speed cell separation: volumetric processing rate (Q) and cell processing rate (measured in cells min^{-1}). This is because

Table 1.1 Direct cell manipulations.

Mechanisms	Techniques	Sample types	Applications	Reported throughput[a)]	Converted throughput Cell counts (cells min^{-1})	References
Electrical	Patch clamp	RAW 264.7, CHO-K1, HIT-T15, and RIN m5F	Recording macroscopic ion channel protein activities	$N = 17$	N/A	[22]
	Impedance spectroscopy	HeLa	Cell impedance measurements	N/A	N/A	[23]
	Impedance spectroscopy	HeLa	Cell impedance response to external chemical perturbations	N/A	N/A	[24]
	Electroporation	K562	Molecule delivery	20 cells per run	N/A	[25]
	Cell lysis	RBC	Lysis	$N = 2\times10^3 - 3\times10^3$	N/A	[26]
	Impedance-based cytometer	3T3	Cell discrimination	1×10^3 cells min^{-1}	1×10^3	[30]
	Impedance-based cytometer	Leukocytes	Cell discrimination	5 µl min^{-1}	5×10^3	[31]
	Impedance-based cytometer	MCF7	Cell discrimination	N/A	N/A	[32]
	Impedance-based cytometer	RBC	Cell discrimination	1×10^3 cells min^{-1}	1×10^3	[33]
	Impedance-based cytometer	RBC	Cell discrimination	N/A	N/A	[34]
	Impedance-based cytometer	Yeast	Subcellular morphology characterization	2 µl min^{-1}	$1\times10^4 - 2\times10^4$	[35]

Optical	Optical stretcher	Myeloid cells	Migration of cells	$N = 44$	N/A	[40]
	Optical stretcher	MCF-7, MCF-10, and modMCF-7	Measuring cell deformability	$N = 83$	N/A	[41]
	Optical stretcher	3T3	Measure the viscoelastic properties of dielectric materials	$N = 20$	N/A	[42]
	Optical stretcher	OKF-4TERT1, OKF-6TERT1, HN, BHY, CAL-27, and CAL-33	Cancer screening	$N = 71$	N/A	[43]
Mechanical	Constriction	RBC	Deformability measurement	$2 \times 10^1 - 2 \times 10^2$ μm s^{-1}	N/A	[59]
	Constriction	RBC	Deformability measurement	N/A	N/A	[60]
Mechanical + electrical	Constriction + electrical	RBC	Deformability measurement	$1 \times 10^2 - 1.5 \times 10^2$ cells s^{-1}	$6 \times 10^3 - 9 \times 10^3$	[53]
	Constriction + electrical	HeLa	Deformability measurement	8×10^2 cells min^{-1}	8×10^2	[54]
Mechanical + optical	Constriction + optical	RBC, H1650, H1975, HCC827, and L1210	Deformability measurement and surface friction of cancer cells	RBC: 1×10^5 cells h^{-1} Others: $\sim 10^3$ cells h^{-1}	N/A	[55]
Mechanical	Constriction	MDA-ME-436 and SUM 1479	Deformability-based separation	$1 - 2$ ml h^{-1}	$1.7 \times 10^4 - 3.3 \times 10^4$	[56]
	Constriction	Leukocytes from whole blood	Deformability-based separation	$1.27 \times 10^1 - 1 \times 10^2$ ml h^{-1}	N/A	[62]
	Constriction	UC13 from leukocytes	Deformability-based separation	9×10^5 cells h^{-1}	1.5×10^4	[63]

(*continued overleaf*)

Table 1.1 (*Continued*)

Mechanisms	Techniques	Sample types	Applications	Reported throughput[a)]	Converted throughput Cell counts (cells min^{-1})	References
	Shear-induced	RBC	Deformability measurement	10 µl min^{-1}	1×10^3	[65]
	Shear-induced	RBC	Characterizing RBC traveling motion	3 µl min^{-1}	N/A	[66]
	Shear-induced	RBC	RBC biophysical property characterization under shear flow	$N = 65$	N/A	[67]
	Shear-induced (inertia)	Leukocytes, malignant pleural cells, and pluripotent stem cells	Deformability-based cytometer	2×10^3 cells s^{-1}	1.2×10^5	[73]
	Shear-induced (inertia)	Malignant pleural effusions (patients' sample)	Deformability-based cell identification	1×10^3 cells s^{-1}	6×10^4	[74]
	Shear-induced (inertia)	HeLa and Jurkat	Deformability-based cytometer	6.5×10^4 cells s^{-1}	3.9×10^6	[57]
	Shear-induced (inertia using non-Newtonian fluid)	RBC and Human Mesenchymal Stem Cells (hMSC)	Deformability measurement	12 µl h^{-1}	6.6×10^3	[58]

a) N stands for maximum number of cells for particular measurements.

limiting the definition of "high speed" to solely one or the other could potentially mislead the figure of merit of an approach. For techniques dealing with blood samples, the throughput will be converted into whole blood processing rate. High speed is defined for techniques with a whole blood processing rate greater than 1 μl min^{-1}. Regarding cultured cells or RBC-free samples, devices capable of processing greater than 10^6 cells min^{-1} are considered high-speed techniques. In the following sections, we discuss two major microfluidic techniques that can separate various cellular types based on hydrodynamic (Section 1.3.1.1) and non-hydrodynamic methods (Section 1.3.1.2). Note that other general cell separation approaches can be found elsewhere [80–87].

1.3.1.1 Hydrodynamic (Passive) Cell Separation

Current state-of-the-art cell manipulation systems can be categorized into passive and active methods depending upon the presence of an external force. Regarding passive systems, the ability to manipulate cells without the aids of external forces allows for simple and cost-effective detection. Various intrinsic biophysical properties, such as cellular size, deformability, and shape, have been exploited to classify different subpopulations of cells via hydrodynamic approaches. In the following sections, we describe recent advances in high-speed microfluidic devices that are capable of purifying cells based on the interactions between cellular biophysical properties and fluid as one of the indirect cell manipulation methods.

Size-Based Cell Separation

Blood is the most complex and information-rich media revealing general patient health and various disease progressions [64]. Thus, the ability to analyze "large" blood volumes (on the order of milliliters) precisely in a "high-speed" manner is a critical task. Surprisingly, there are not so many microfluidic platforms capable of processing whole blood (i.e., undiluted blood) or samples with a very high hematocrit level [21, 88–95]. Among them, one successful cell separation method that should be highlighted is deterministic lateral displacement (DLD)-based platforms [96, 97]. Briefly, when cells (or particles) travel through an array of microposts in DLD systems, cells with a diameter greater than the critical dimension collide more with microposts, laterally deflecting their path perpendicular to the primary flow. On the other hand, cells below the critical dimension stay within their initial streamlines. Cell migration motions are not random and can be tuned precisely based on the critical dimension determined by micropost geometry, channel and cell dimensions, and other arrangements [98]. DLD has been widely used for blood cell fractionation, rare cell detection, and RBC removal before performing additional downstream biological assays [97]. For example, Inglis *et al.* [92] demonstrated a buffer-free DLD platform for leukocyte enrichment from whole blood. Significantly high whole blood processing rates of 115 μl min^{-1} (9.5×10^6 cells s^{-1}) were reported. Later, Loutherback *et al.* [99] purified rare cancer cells from diluted bloods with an increased throughput of 2.5×10^9 cells min^{-1}. As shown in Figure 1.3a, the platform uses triangular posts over conventional circular microposts, providing a more efficient and clog-free operation. Liu

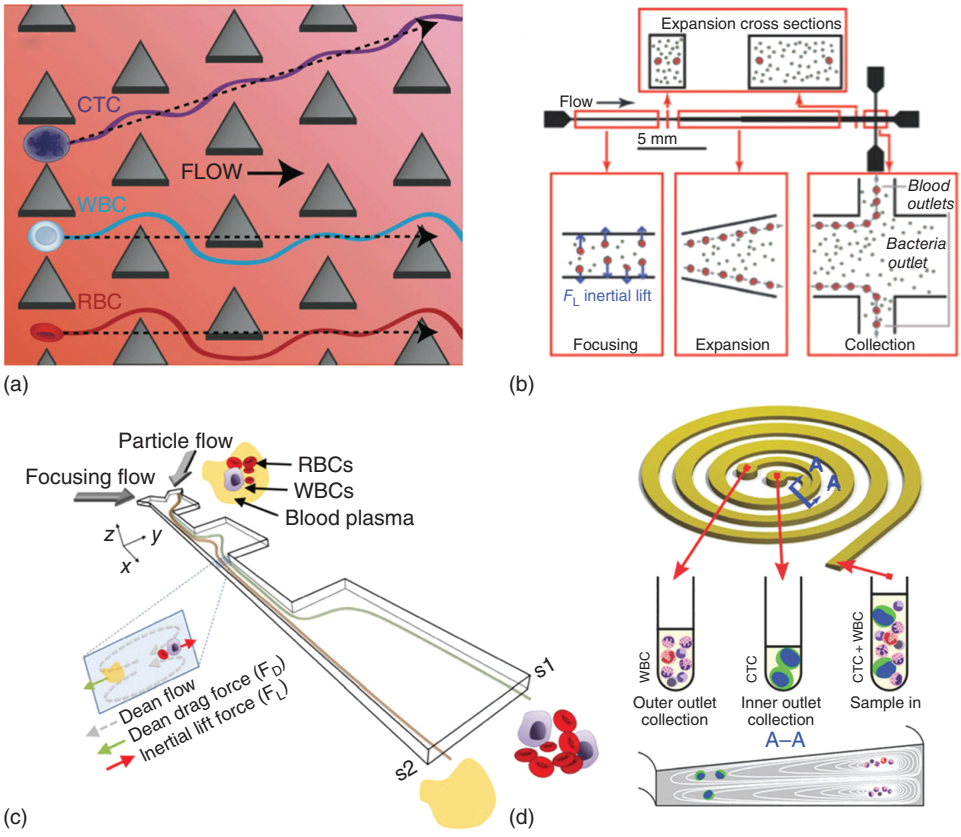

Figure 1.3 Indirect hydrodynamic size-dependent cell separation systems. Cells with various sizes experience different magnitudes of hydrodynamic forces, inducing lateral migrations, when they are flown through (a) arrays of microposts [99], (b) a straight microchannel [100], (c) a microfluidic channel with series of contracting and expanding geometries [91], or (d) spiral microchannels [89]. As the modification degree of lateral migrations is strongly influenced by cellular sizes, various cell types can be separated downstream.

et al. [101] also used a triangular micropost array enriching various cancer cell lines from diluted peripheral whole blood with a maximum throughput of 2 ml min^{-1}.

Even though DLD-based techniques hold great promise for high-speed blood purification, fluid inertia-based microfluidic devices have been investigated to reach higher throughputs. Inertial effects in microfluidic systems have recently been recognized as a robust way of manipulating microscale particles because they fundamentally offer high-speed sample processing, simple operation, precise cell manipulation, and a great potential for automation and miniaturization [70, 71]. As we briefly mentioned in Section 1.2.4.2, there are two types of inertial

effects: inertial particle migration and secondary flow, which can be exploited for cell separations as well. At finite Reynolds numbers, the flowing cells/particles experience two directional lift forces: shear-gradient lift forces and wall-effect lift forces. Broadly speaking, a balance of these two counteracting lift forces results in cell migrations across streamlines [70–72]. For a square channel, due to the channel's fourfold symmetry, particles or cells migrate toward midpoints of the four channel walls, forming four particle/cell chains. Research findings showed that these lift forces vary with cell diameter, deformability, channel geometry, and flow conditions [70–72]. The magnitudes of the lift forces strongly correlate with cell sizes ($F_L \propto \rho U^2 a^4/H^2$) [102]; therefore, cells with large size differences will have distinctive lateral positions. For example, larger cells focus close to the channel center whereas smaller ones focus closer to the wall. As shown in Figure 1.3b, Mach and Di Carlo [100] separated bacterial cells from blood with a throughput of 4×10^8 cells min^{-1} based on cell size difference. It should be noted that the equilibrium positions of two distinct cell sizes are relatively close; therefore, additional efforts on modifying channel designs, such as gradually expanding channel widths [100] or inverting channel aspect ratios [103], have been implemented to enhance separation efficiency.

Periodic channel geometry variations also have been used to develop size-based cell separation devices. As shown in Figure 1.3c, microchannels with a series of contractions and expansions are implemented to separate cells based on their sizes. As cells flow through the device, they periodically experience inconsistent lift forces depending upon the presence of the wall, and the net force directs cells with larger diameter closer to the channel wall. Using this mechanism, greater than 10^7 cells min^{-1}, equivalent to processing whole blood at 2 μl min^{-1} or more, were processed for CTC purification [91, 104–106]. A similar channel layout can be used to trap cells in microvortices created in the expansion regions [107–110]. With an absence of channel wall in the vicinity of cellular flow paths at expansion regions, cells are exposed to a dominant shear-gradient lift force. Since bigger cells experience a larger shear-gradient lift force, they were more prone to be pushed and trapped inside the microvortices formed in expansion chambers. Using this vortex cell trapping mechanism, CTC purification has been demonstrated with throughputs ranging from 5×10^8 to 4×10^9 cells min^{-1}, equivalent to processing whole blood from 114 to 490 μl min^{-1} [107–110].

The other major inertial effect found in microchannels utilizes a secondary flow. In a curved channel, fluid elements in the center travel faster than those near the channel walls due to momentum mismatch, creating a pair of secondary flow known as *Dean flow* [111]. Dean flow exerts an additional hydrodynamic force, namely Dean drag force, and cells with varying sizes experience different net forces (a sum of Dean drag, Stokes drag, wall-effect, and shear-gradient lift forces), resulting in size-based lateral equilibrium positions. Dean flow-based cell manipulation is a powerful method offering extremely high throughputs for CTC purification, blood cell fractionation, and cell cycle synchronizations with throughputs ranging from 2.5×10^5 to 2.5×10^8 cells min^{-1} [90, 94, 112–119]. As shown in Figure 1.3d, trapezoidal cross-sectional shapes of spiral channels are reported

[89, 120, 121], allowing higher separation efficiency for enriching CTCs with a throughput from 7.5 ml of patients' blood samples (lysed blood) within 8 min, equivalent to 6.6×10^5 cells min^{-1} [89, 90].

Inertial focusing, in general, operates with diluted samples to minimize inter-particle interactions [122] while maximizing purity and efficiency. However, their inherently fast operating flow speeds allow superior throughputs (greater than a few million cells per minute, equivalent to a few microliters of whole blood per minute). Furthermore, the simple microchannel design of inertial focusing devices allows further enhancement of throughput by parallelizing [100] or stacking [118] the single channels.

Deformability-Based Cell Separation

Cells can be purified using their intrinsic stiffness, and much effort has been made on investigating RBC deformability. Regarding RBC deformability-based separation, a hydrodynamic lift, scaling with deformability of the RBCs, induces migration of soft RBCs toward the center of the channel, creating a cell-free layer near the wall, and the phenomenon is known as *Fåhraeus–Lindqvist effect* (*a.k.a. Sigma effect*) [123]. As shown in Figure 1.4a, Faivre *et al.* [88] explored the variations of RBC rheology affecting cell-free layer widths based on hematocrit counts, flow speeds, and constriction geometries. They were able to purify a plasma-rich solution from threefold diluted blood at the processing rate of 17 µl min^{-1}. Sollier *et al.* [127] exploited the recovery time in which RBCs return to their initial positions after passing a contraction to extract plasma with a processing rate of 5 µl min^{-1}using 20-fold diluted blood. Jain *et al.* [128] has utilized a straight microfluidic channel with sudden expansion geometry to extract stiffer white blood cells (WBCs) from twofold diluted whole blood with a processing rate of 14 µl min^{-1}. Using a similar phenomenon, Hou *et al.* [95] demonstrated that more stiff malaria-infected erythrocytes can be filtered from the normal blood cells using a straight microfluidic channel. The device can be operated using whole blood and was capable of processing at 5 µl min^{-1}.

In order to achieve higher throughputs, deformability-based cell separation was demonstrated via inertial microfluidics. Deformable particles have modified lateral equilibrium positions compared to their rigid counterparts with similar sizes because they experience an additional lift force, ascribed to nonlinear mismatch of velocities and stresses at the interface [129]. As the magnitude of deformability-induced lateral force scales with cellular softness, cells with a different deformability value can be used for separation. For example, softer cells can be found closer to the channel center where the shear stress is at the minimum whereas stiff cells remain close to the channel wall. As illustrated in Figure 1.4b, separating cancer cells spiked in lysed blood has been demonstrated using combined effects of the inertial focusing and the deformability-induced cell migration [124]. The inherently high flow rates allowed purification of more deformable and larger cancer cells from the lysed blood with a throughput of 22 000 cells min^{-1}, equivalent to processing 3 µl of whole blood per minute [124]. This value is more than a 40-fold improvement over that of previous cell

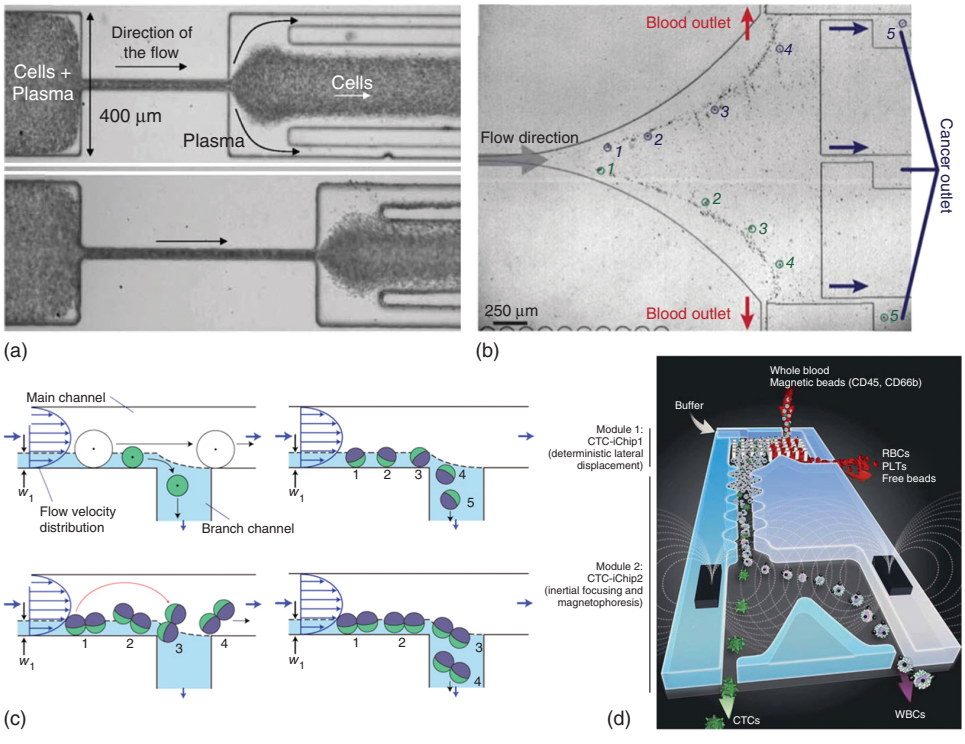

Figure 1.4 Separation of various cell types based on (a,b) cellular deformability, (c) shape, and (d) combination of multiple distinguishing markers. Lateral positions of cells with various deformability can be differentially manipulated by using (a) geometrical constrictions [88] as well as (b) deformability-induced lift forces [124]. (c) Effective diameters of tumbling nonspherical cells tend to be larger than their actual length, allowing shape-based cell separations [125]. (d) Systems capable of processing large volumes of cellular samples can be integrated upstream of conventional affinity-based cell sorting techniques [126].

purification techniques utilizing the hydrodynamic lift force alone [130]. These deformability-based cell separation techniques hold great promise for simple and cost-effective target cell purification systems for cells with little-to-no known surface biomarkers.

Shape-Based Cell Purification

Similar to size and deformability, the shape can serve as a unique cell separation parameter for various biological particles and organisms. The use of the aforementioned DLD techniques was expanded for shape-based cell sorting [131]. In particular, parasites were purified from the infected blood since the long parasites' morphology result in a larger effective size, causing them to deflect across streamlines, while smaller RBCs faithfully remain in their initial streamlines [93]. They processed twofold diluted blood with a flow rate of 60 µl min^{-1}.

The shape-based separation was also implemented to purify subpopulations from yeasts and tissue digests. Inertial focusing of nonspherical particles has been examined, and it was found that, for nonspherical but symmetric particles, the rotational diameter that the particles create as they tumble determines their lateral location in the channel [132]. Utilizing this characteristic, budding yeasts were purified based on their elongated lengths, synchronized with their cell cycle [133]. They processed the sample at the rate of 60 µl min^{-1} equivalent to 90 000 cells min^{-1}. Moreover, differences in lateral equilibrium positions of nonspherical multicellular clusters of mature somatic cells and smaller spherical progenitor cells were utilized for adrenal cortical progenitor cell enrichment [134].

Similar to inertial focusing of nonspherical particles [132], elongated budding yeasts create a larger rotational trajectory as they tumble through the hydrodynamic filtration systems, making them behave like spherical particles with a larger diameter (see Figure 1.4c). Utilizing the enlarged effective diameter of budding yeast, Sugaya *et al.* [125] separated nonspherical budding yeasts from their smaller counterparts with a throughput of 1.5×10^6 cells min^{-1}. Shape-based cell separation techniques suggest a new paradigm for target cell enrichment strategies in various biological applications (Table 1.2).

1.3.1.2 Nonhydrodynamic (Active) Particle Separation

Nonhydrodynamic bioparticle separation utilizes external forces. In general, separation is achieved by deflecting cells' lateral position in response to external stimuli, such as acoustic, electric, optic, and magnetic forces, whose magnitudes vary with cellular properties. We describe individual cell separation mechanisms for various nonhydrodynamic methods and mainly highlight high-speed methods in this section. We also tabulate each nonhydrodynamic particle separation in Table 1.3. More general indirect cell separation approaches can be found elsewhere [81, 84, 135–137].

Acoustic Cell Separation

Acoustic cell manipulation utilizes acoustic waves transduced by applied electric fields on piezoelectric materials [138]. Typical layouts consist of piezoelectrics patterned on the substrate and a microfluidic channel. The radial acoustic force acting on a particle is given by

$$F_r = -\left(\frac{\pi p_0^2 V_p \beta_m}{2\lambda}\right)\left(\frac{5\rho_p - 2\rho_m}{2\rho_p + \rho_m} - \frac{\beta_p}{\beta_m}\right)\sin(2kx), \tag{1.1}$$

where p_0 is the pressure amplitude, V is the particle volume, β is the compressibility, λ is the ultrasound wavelength, ρ is the density, and k is the wave number. Subscripts "p" and "m" denote the particle and the fluid medium, respectively [139, 140]. Normally, particles or cells are transported in either pressure nodes or antinodes depending upon their properties, allowing various cell patterning. For example, both point and linear cell alignments can be

Table 1.2 Indirect cell manipulations: hydrodynamic separation.

Mechanisms	Techniques	Sample types	Applications	Reported throughput	Converted throughput			References
					Whole blood ($\mu l\ min^{-1}$)	Flow rate ($\mu l\ min^{-1}$)	Cell counts ($cells\ min^{-1}$)	
Hydrodynamic: Size	Slanted spiral inertial focusing	Lysed blood + cancer cells, lysed patient's samples	CTC purification	7.5 ml/8 min	938	1700	6.6×10^5	[89]
	Slanted spiral inertial focusing	Lysed blood + cancer cells, lysed patient's samples	CTC purification	7.5 ml/8 min	938	1700	6.6×10^5	[90]
	CEA	Whole blood + cancer cells	CTC purification	1.1×10^8 cells min^{-1}	5	6000	1.1×10^8	[91]
	DLD	Whole blood cells	Blood fractionation	115 $\mu l\ min^{-1}\ atm^{-1}$	115	115	5.9×10^8	[92]
	DLD	Diluted blood + cancer cells	CTC purification	5 $ml\ min^{-1}$	500	5000	2.5×10^9	[99]
	DLD	Diluted blood + cancer cells	CTC purification	2 $ml\ min^{-1}$	200	2000	1×10^9	[101]
	Inertial focusing	Diluted blood + bacterial cells	Sepsis filtration	4×10^8 cells min^{-1}	2.2	200	4×10^8	[100]
	Inertial focusing	Diluted blood + cancer cells	CTC purification	100 $\mu l\ min^{-1}$	1.8	100	8.9×10^6	[103]
	CEA + Steric filters	Diluted blood + cancer cells	CTC purification	130 $\mu l\ min^{-1}$	2.9	130	1.4×10^7	[104]
	Pinched Flow	Diluted blood + cancer cells	CTC purification	400 $\mu l\ min^{-1}$	18	400	8.9×10^7	[105]
	Multi-orifice	Diluted blood + cancer cells	CTC purification	126 $\mu l\ min^{-1}$	1.3	126	6.3×10^6	[106]
	Vortex trapping	Diluted/lysed blood + cancer cells	CTC purification	7.5×10^6 cells s^{-1}	114	4000	4.5×10^8	[107]

(*continued overleaf*)

Table 1.2 (*Continued*)

Mechanisms	Techniques	Sample types	Applications	Reported throughput	Converted throughput			References
					Whole blood ($\mu l\ min^{-1}$)	Flow rate ($\mu l\ min^{-1}$)	Cell counts (cells min^{-1})	
	Vortex trapping	Diluted blood + cancer cells	CTC purification	4.4 ml min^{-1}	489	4400	2.4×10^9	[108]
	Vortex trapping	RBC-lysed pleural samples (patient's samples)	CTC purification	50 ml/10 min	NA	6000	NA	[109]
	Vortex trapping	Diluted patient's samples	CTC purification	7.5 ml/20 min	375	4000	3.6×10^9	[110]
	Asymmetric curve inertial focusing	Diluted blood	Blood fractionation	1 ml min^{-1}	22	1000	1.1×10^8	[112]
	Symmetric curve inertial focusing	Diluted blood + murine cancer cells	Cell separation/CTC purification	600 $\mu l\ min^{-1}$	6	600	3×10^7	[113]
	Multistage inertial focusing + Dean force	Diluted blood + cancer cells	CTC purification	565 $\mu l\ min^{-1}$	13	565	6.3×10^7	[114]
	Spiral inertial focusing with sheath fluid	Diluted/lysed blood + cancer cells or patient's samples	CTC purification	100 $\mu l\ min^{-1}$	50	100	2.5×10^8	[94]
	Spiral inertial focusing	Diluted blood	Blood fractionation	1×10^6 cells min^{-1}	2.2	1000	1×10^6	[115]
	Spiral inertial focusing	Cancer cells	Cell separation	1×10^6 cells min^{-1}	NA	3000	1×10^6	[116]
	Spiral Inertial Focusing	Mesenchymal stem cells	Cell cycle synchronization	2.5×10^5 cells min^{-1}	NA	2500	2.5×10^5	[117]

	Stacked spiral inertial focusing	Lysed patient's samples	CTC purification	7.5 ml/5 min	1500	NA	1.1×10^7	[118]
	Double spiral inertial focusing	Diluted blood + cancer cells	CTC purification	3.3×10^7 cells min^{-1}	20	333	3.3×10^7	[119]
	Slanted spiral inertial focusing	Diluted blood	Blood fractionation	0.8 ml min^{-1}	10	800	5×10^7	[121]
Hydrodynamic: Deformability	Expansion/ contraction	Diluted blood	Blood fractionation	1 ml h^{-1}	5.9	17	3×10^7	[88]
	Lateral migration	Diluted blood	Blood fractionation	100 µl min^{-1}	5	100.00	4.7×10^7	[127]
	Expansion	Diluted blood	Blood fractionation	1×10^4 cells μl^{-1} at $\gamma = 400\ s^{-1}$	6.8	13.5	1.4×10^5	[128]
	Lateral migration	Healthy + infected RBC	Malaria-infected RBC purification	5 µl min^{-1}	5	5	2×10^7	[95]
	Inertial focusing	Lysed blood + cancer cells	CTC purification	2.2×10^4 cells min^{-1}	3.14	60	2.2×10^4	[124]
	Hydrodynamic lift	Dilute blood + cancer cells	CTC purification	20 µl h^{-1}	0.07	0.33	6.3×10^5	[130]
Hydrodynamic: Shape	DLD	Whole blood + parasites	Infection detection	600 µm s^{-1}	1	60	3×10^8	[93]
	Inertial focusing	Budding yeast	Cell cycle synchronization	60 µl min^{-1}	NA	60	9×10^4	[133]
	Inertial focusing	Tissue digest	Stem cell purification	60 µl min^{-1}	NA	60	2.4×10^4	[134]
	Hydrodynamic filtration	Budding yeast	Cell cycle synchronization	15 µl min^{-1}	NA	15	1.5×10^6	[125]

achieved by modulating system parameters, such as acoustic wavelength and the cells' density, deformability, and size. Point or linear cell alignment is a powerful technology to manipulate multiple cells, and recently Ding *et al.* [141] developed acoustic tweezers using surface acoustic waves, demonstrating active cell and organism transport. However, since cells were trapped in spatially defined nodes, the technique has limited throughput. For high-throughput applications, acoustic waves have been used for cell sorting. As can be seen in Eq. (1.1), the radial acoustic force varies with different or cell-specific parameters. For example, RBCs, platelets, and leukocytes were successfully discriminated depending on their size [142] or size with density [143]. Yang *et al.* [144] also demonstrated separation of viable breast cancer cells (MCF7) from nonviable counterparts based on their volumetric differences. Toward higher throughput, Adams *et al.* reported separation of RBCs from whole blood by applying an acoustic wave in the vertical direction without the use of a burdensome sheath fluid (see Figure 1.5a). The sample processing rate reached as high as $2\,l\,h^{-1}$ as one of the fastest processing methods [145]. Acoustophoretic cell manipulation techniques provide many advantages including high-speed, label-free, simple, noninvasive, precise, and tunable cell manipulations.

Electrical Cell Separation

Dielectrophoresis (DEP) is a representative electrical cell manipulation technique that relies on the Coulomb response of polarized cells or particles exposed to a nonuniform electrical field [149]. The time average force acting on a dielectric micro-object can be expressed as follows:

$$F_{\mathrm{DEP}} = 2\pi\varepsilon_{\mathrm{m}} r^3 f_{\mathrm{CM}}(\nabla E^2), \tag{1.2}$$

where ε_{m} is the absolute permittivity of the medium, r is the radius of the micro-object, f_{CM} is the Clausius–Mossotti (CM) factor, and E is the root mean square (RMS) amplitude of the electrical field. The derivation of Eq. (1.2) and the theoretical background can be found elsewhere [149, 150]. By modifying various parameters listed in Eq. (1.2), one can precisely predict and control overall cell behavior and motions in the solution. Depending on the relative permittivity values between cells and the medium, the direction that cells migrate can be reversed. Cells can be transported toward a region of either stronger (positive DEP; higher polarization of micro-objective compared to medium) or lower electrical field (negative DEP; smaller polarization of micro-objective than medium) regions. Note that the DEP force is directly proportional to the square of the applied electrical field; therefore, both AC and DC fields can be used for cell manipulations [151].

The general approach is that cells flow in microchannels with electrodes patterned on the substrate. Once cells approach to the electric field region, they are laterally deflected. The degree of cell migration varies with electrical properties and other parameters (see Eq. (1.2)). Mammalian [152–156] and bacterial cells [157] were successfully classified based on cell volume ($F_{\mathrm{DEP}} \propto r^3$). It should be noted that DEP-based cell manipulation methods have not been well

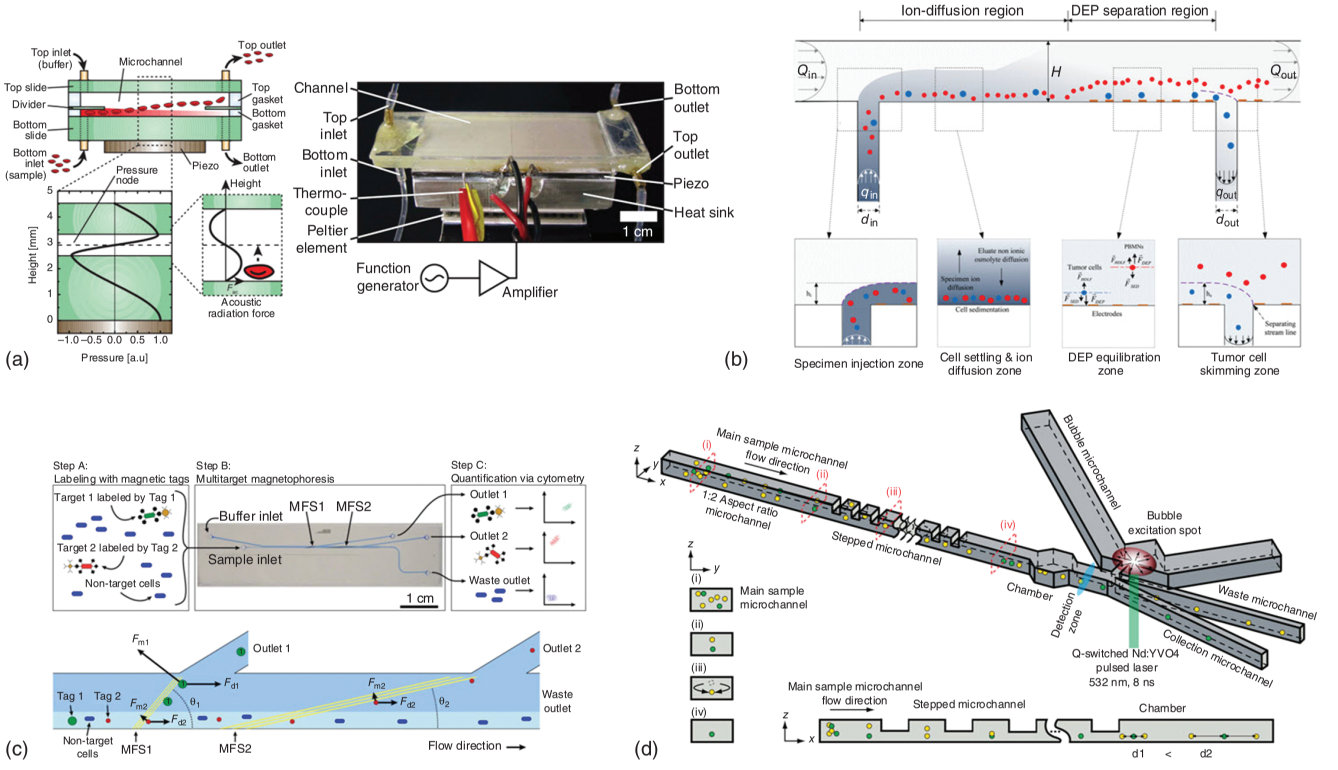

Figure 1.5 Nonhydrodynamic cell manipulation techniques (a–c) and cell alignment (d). (a) Acoustic force deflected RBCs selectively for RBC separation [145]. (b) Circulating tumor cells are displaced vertically by dielectrophoretic force from peripheral blood mononuclear cell (PBMN) [146]. (c) Magnetically tagged cells are sorted in response to the degree of magnetic forces [147]. (d) AB3955 cells are inertially focused and classified upon their fluorescence signals [148].

favored for high-speed cell separation because of the relatively low-throughput cell ($<10^6$ cells min^{-1}) processing limit. However, recently, Shim *et al.* [146] reported a promising DEP chip with a high processing rate of 10 ml h^{-1} (equivalent to 4×10^7 cells min^{-1}) as shown in Figure 1.5b. Even though pure whole blood was not processed and device fabrication was not trivial, it showed precise, continuous, and label-free cell manipulation with a high processing rate.

Magnetic Cell Separation

The ability to sort cells using magnetic forces has been extensively utilized for cell separation. Magnetophoresis can be achieved by utilizing intrinsic cell magnetization or cell functionalization with magnetic elements. For instance, deoxyhemoglobin RBCs can be naturally magnetized under applied magnetic fields, and label-free separation of RBCs from whole blood was demonstrated [158]. However, due to their weak response to magnetic fields, impractically high magnetic fields should be applied to improve separation efficiency. Therefore, magnetic element labeling is more preferred rather than exploiting natural magnetism. The magnetic force acting on a particle can be written as

$$\vec{F}_{\mathrm{M}} = \frac{V\chi}{\mu_{\mathrm{o}}}(\vec{B}.\nabla)\vec{B}, \tag{1.3}$$

where V is the volume of the magnetic particle, χ is the magnetic susceptibility, μ_{o} is the magnetic permeability in vacuum, and $\vec{B}$ is the magnetic field [37]. In general, magnetically labeled cells are injected into microfluidic channels, and an external magnetic source is used to deflect cell lateral positions based on their magnetic responses [36]. The magnetic-activated cell sorter (MACS) is a prime example of a high-speed cell separation technique ($>10^7$ cells min^{-1}) [159]. Normally, cells are conjugated with magnetic nanoparticles whose surfaces are coated with antibodies binding to antigens expressed on target cells. As shown in Figure 1.5c, Adams *et al.* [147] used MACS-based multimagnetic tagging methods differentiating different bacterial cell types with a throughput of 10^9 cells h^{-1}. The MACS mechanism was also used to purify living fungal pathogens bound to magnetic particles covered with opsonins from whole blood at a processing rate of 20 ml h^{-1} [21] (see Figure 1.1b). Even though the time to process cells in microfluidic devices is short, a nontrivial and lengthy sample preparation step is required for magnetic cell manipulations.

Instead of tagging magnetic elements on cell surface, endocytosis of magnetic nanoparticles can be used to indirectly manipulate cellular positions in flow [160]. Depending on endocytotic capacity of magnetic nanoparticles, cells showed a different degree of magnetic responses. Robert *et al.* [161] recently demonstrated separation of monocytes and macrophages based on amounts of internalized magnetic nanoparticles. Even though the use of internalization-based approach is limited because of its relatively low cell processing rate (10–100 cells s^{-1}) and high cytotoxicity of nanoparticles [162], this approach opened a door for integrated cell manipulations as a future direction. For example, internalized

nanoparticles can be used for enhanced imaging, hyperthermia, and controlling local cell motions and mitoses [163].

Optical Cell Separation

Cell sorting exerted by optical forces has also been employed for cell separation. Optics-based cell separation was shown using cellular optical characteristics, such as refractive index [164] or light patterns [165]; however, similar to direct cell manipulations, most techniques still exhibit extremely limited processing rates. Regarding high-throughput cell separation applications, microfluidic fluorescence-activated cell sorter (FACS) is one of the major optical cell sorting examples [166]. Briefly, a stream of cells exiting a capillary tube breaks into individual droplets, and droplet trajectories are deflected laterally upon their fluorescence (i.e., charge) responses to the applied external field. FACS throughput reaches as high as 50 000 cells s^{-1}, analyzing cells rapidly; however, it should be noted that fluorescent labeling should be done before cell interrogation, and the processing rate is still not high enough for rare cell detections [167]. Note that flow cytometry is discussed in Section 1.3.2.1 separately.

Hybrid Cell Purification Systems

There have been innovative attempts to develop a new cell manipulation method by combining multiple cell manipulation techniques together to enhance their performance. The most commonly integrated technique with other modalities is magnetophoresis because it allows to selectively deflect labeled cells attained upstream by other indirect cell manipulation methods. DLD and magnetophoresis were combined to purify CTCs from patients' blood samples [126, 168]. DLD-based platforms were used to exhaust overly populated RBCs from the whole blood, and magnetophoresis were subsequently used to deflect the flowing path of magnetically labeled WBCs (see Figure 1.4d). This hybrid system was able to process 150 µl of whole blood per minute, showing great potential for practical CTC detections. Magnetophoresis was also incorporated with the hydrodynamic filtration technique [169]. They first guided HeLa and Jurkat cells based on their sizes toward outlets, and those separated cells' streams were further branched out based on the expression level of CD4 with a throughput of 6000 cells min^{-1}. There exist other innovative hybrid cell separation techniques that are not discussed here due to their low operational speeds, but more details can be found elsewhere [170–172] (Table 1.3).

1.3.2 Cell Alignment (Focusing)

Along with cell separation, another key cell path manipulation method is cell alignment (focusing). In this section, cell alignment/focusing is defined as the phenomena forming a cell train/chain(s) as they travel downstream. Cell focusing also can be achieved by exposing flowing cells to either hydrodynamic forces (active) or nonhydrodynamic forces (passive). Cell focusing is an extremely

Table 1.3 Indirect cell manipulations: nonhydrodynamic separation.

Mechanisms	Techniques	Sample types	Applications	Reported throughput	Converted throughput	References
					Cell counts (cells min^{-1})	
Acoustic: size	Acoustophoresis	Whole blood	Cell separation	2.7×10^4 cells s^{-1}	1.6×10^6	[142]
Acoustic: size/density	Acoustophoresis	Diluted blood	Cell separation	0.76 ml min^{-1}	4.9×10^9	[143]
Acoustic: size	Acoustophoresis	Cancer cells	Cell separation	12 ml h^{-1}	2×10^5	[144]
	Acoustophoresis	Whole blood + microparticles	Cell separation	2 l h^{-1} (whole blood)	N/A	[145]
Electrical: density and dielectric properties	Dielectrophoresis	Lysed blood	Cell separation (leukocytes subpopulation)	0.2 ml min^{-1}	4×10^5	[152]
Electrical: size and dielectric properties	Dielectrophoresis	Diluted blood + cancer cells	CTC detection	1.5–12 ml min^{-1}	3×10^2–6×10^4	[153]
Electrical: size	Dielectrophoresis	Diluted blood	Cell separation	1 mm s^{-1}	1–2×10^4	[154]
Electrical: size (volume)	Dielectrophoresis	Cancer cells	Cell separation (cell cycle based)	2×10^5 cells h^{-1}	3.3×10^3	[155]
Electrical: size	Dielectrophoresis	Diluted blood + cancer cells	Cell separation	0.1–0.5 ml h^{-1}	N/A	[156]
	Dielectrophoresis	Bacterial cells + diluted blood or cerebrospinal fluid	Cell separation	330 µl h^{-1}	1.7×10^3	[157]
	Dielectrophoresis	Diluted blood + cancer cells	CTC detection	1×10^6 cells min^{-1}	1×10^6	[146]
Magnetic: natural magnetism	Magnetophoresis	Whole blood	Cell separation	N/A	N/A	[158]

Magnetic labeling	Magnetophoresis	Spleen + myeloma cells	Cell separation	10^9 cells/15 min	6.7×10^7	[159]
	Magnetophoresis	Bacterial cells	Cell separation	10^9 cells h^{-1}	1.7×10^7	[147]
	Magnetophoresis	Fungal cells + whole blood	Pathogen clearance from blood	20 ml h^{-1} (whole blood)	NA	[21]
Magnetic: endocytotic capacity	Magnetophoresis	White blood cells	Cell separation	$1 \times 10^1 - 1 \times 10^2$ cells s^{-1}	$6 \times 10^2 - 6 \times 10^3$	[161]
Optical	Reflective index	N/A	Cell (RBC) separation	N/A	N/A	[164]
	Light pattern	Diluted blood	Cell separation	N/A	N/A	[165]
	Fluorescence	Cancer cells	Cell separation (FACS)	1.06×10^2 cells s^{-1}	6.4×10^3	[166]
Hybrid	DLD + magnetophoresis	Whole blood + cancer cells or patients' sample	CTC purification	1×10^4 cells s^{-1}	6×10^5	[168]
	DLD + magnetophoresis + asymmetric inertial focusing	Whole blood + cancer cells or patients' sample	CTC purification	1×10^7 cells s^{-1}	6×10^8	[126]
	Hydrodynamic filtration + magnetophoresis	Cancer + lymphocyte cells	Cell separation	100 cells s^{-1}	6×10^3	[169]

useful technique preceding additional biological assays [173] because, by accurately positioning the locations of flowing cells in microchannels, sophisticated cell manipulation and higher cell sorting efficiencies can be achieved. Cell alignment has several specific purposes, and we discuss some of their main objectives.

1.3.2.1 Cell Alignment (Focusing) for Flow Cytometry

The most widely explored cell focusing application is flow cytometry. Flow cytometry is a powerful and high-speed analytical tool because it is capable of performing single molecule detection, imaging, counting, analysis, sorting (e.g., FACS), immunophenotyping, and classification of various cellular types [167]. Conventional flow cytometers deliver cells through a thin capillary called a *flow cell* where cells are focused and optically interrogated. Since the sensitivity and specificity of the fluorescent signal detections strongly depend on the proximity of the fluorescent label and laser beam spot, focusing cells upstream is a crucial task. Cells and particles are normally focused hydrodynamically via sheath fluid. As the sheath is delivered with a higher flow rate compared to the core flow speed, the diameter of the cell stream becomes compatible to the size of the interrogation beam spot. Sheath fluid-based cell focusing offers simple and precise three-dimensional cell focusing; however, extremely large volumes of sheath fluid are required to narrow down the cell stream and to process large-volume samples [167]. In order to address this shortcoming, various sheathless cell focusing [173] methods are reported for next-generation flow cytometers. Among those, we discuss here high-speed and simple sheathless cell focusing techniques, particularly inertial focusing and acoustophoresis.

As discussed in Section 1.2.4.2, at finite Reynolds numbers, inertial lift forces can be utilized to position cells and particles precisely in a predictable manner [70–72]. Since inertial focusing creates multiple cell/particle chains across the channel cross section (e.g., two, four, or more depending on channel shape, flow speed, and aspect ratio) [70–72], Dean flow has been implemented to create a single-cell stream [174, 175]. Solely utilizing fluid inertia to focus particles, flow cytometer applications were successfully demonstrated [176, 177]. Recently, single-stream cell focusing was also achieved in straight microchannels containing columns. The platform exploited inertial flows induced by interactions between fluid and channel structure [178, 179], and its applicability as FACS was demonstrated with a throughput of 6×10^5 cells min^{-1} processing lymphoma cells [148] (see Figure 1.5d). As another inertial approach, Hur *et al.* [180] used a high-aspect ratio channel, creating two cell chains and positioning all cells in a single focal plane. By massively parallelizing microchannels, an ultrahigh throughput (10^6 cells s^{-1}) image cytometer was reported. Inertial particle focusing mechanism strongly depends on particle sizes so that it still remains a challenge to design a universal microfluidic channel that focuses various cell sizes; nevertheless, because of its simple and passive mechanism and rapid processing rate, inertial focusing holds a great promise.

Another cell focusing approach is through acoustophoresis. Standing surface acoustic wave (SSAW)-based microfluidic cytometers [181–183] and acoustic actuated fluorescence-activated sorting of microparticles were demonstrated [184] by utilizing the interactions between acoustic waves and cells. Moreover, there are several commercially available flow cytometers adopting acoustophoresis in combination with hydrodynamic focusing [167, 185]. Compared to passive cell focusing methods, the acoustic wave-based cell focusing technique relies on an external apparatus; therefore, the approach requires relatively more complicated fabrication procedures. However, as discussed in section "Acoustic Cell Separation", acoustophoresis offers label-free, rapid, simple, noninvasive, precise, and tunable cell manipulations, posing itself as one of the most promising candidates for flow cytometry.

1.3.2.2 Cell Solution Exchange

High-speed cell alignment can be used for rapid solution exchange by manipulating cell flow paths. Solution exchange steps are frequently conducted to label and wash cells for downstream imaging and analysis [186]. Centrifugation is the easiest and most common approach to isolate cells from complex backgrounds; however, it is slow and labor-intensive, and sample loss during the recovery step is inevitable [18]. In order to address these shortcomings, Gossett *et al.* [187] reported a novel microfluidic platform named Rapid Inertial Solution Exchange (RInSE), exploiting inertial cell migration. Through a modulation of channel aspect ratio, cell lateral positions were manipulated, extracting cells from one stream to the other. In short, leukocytes were inertially transferred into a solution of phosphate buffered saline (PBS) from a lysed whole blood sample with a throughput of 1000 cell s^{-1} and 96% efficiency. This approach was expanded later for automated continuous cytomorphological staining [188] and time-controlled transient chemical treatment of cells (on the order of 1 ms) [189]. It is true that large output volumes were induced, requiring a further concentration step; nonetheless, the method offers high-speed cell process with very high efficiency. As another cell solution exchange, platforms utilizing microvortices were reported. The typical channel geometry consists of a straight microchannel with a series of expansion–contraction chambers (see section "Size-Based Cell Separation" for the detailed mechanism). While cells were trapped in recirculating microvortices in the expansion chambers, new solutions were injected for solution exchange. Mach *et al.* [108] demonstrated various cell labeling with antibodies to intracellular components (cytokeratin), cell surface proteins epithelial cell adhesion molecule (EpCAM), fluorogenic enzyme substrates (Calcein AM), and direct labeling of DNA 4′,6-diamidino-2-phenylindole (DAPI). It should be noted that microvortices-based solution exchange does not require any postconcentration step as compared to RInSE, but the number of cells that can be processed simultaneously is predetermined and inflexible (Table 1.4).

Table 1.4 Indirect cell manipulations: cell alignment.

Mechanisms	Techniques	Sample types	Applications	Reported throughput (cells s^{-1})	Converted throughput	References
					Cell counts (cells min^{-1})	
Hydrodynamic	Inertial particle focusing + geometry-induced secondary flow	Cancer and leukemia cells	Focusing/flow cytometer	3.4×10^4	2×10^6	[178]
	Inertial particle focusing + geometry-induced secondary flow	Cancer and leukemia cells	Focusing/flow cytometer	1.3×10^4	7.8×10^5	[179]
	Inertial particle focusing + geometry-induced secondary flow	Lymphoma cells	Focusing/FACS	1×10^4	6×10^5	[148]
	Inertial particle focusing	Diluted blood	Cell counting	1×10^6	6×10^7	[180]
Acoustic	Acoustophoresis	Cancer cells	Cell counting	1×10^3	6×10^4	[181]
Hydrodynamic	Inertial particle focusing	Lysed blood	Solution exchange	1×10^3	6×10^4	[187]
	Inertial particle focusing	Cancer cells	Cytomorphological staining	N/A	N/A	[188]
	Inertial particle focusing	Cancer cells	Transient chemical treatments	N/A	N/A	[189]

1.4 Summary

We have discussed various microfluidic techniques for cell manipulation, and "high-speed" cell manipulations are successfully achieved with various approaches. Each technique has its own advantages and disadvantages, and sometimes hybrid approaches provide more cellular information. Depending on biological questions, one should decide which technique would be the most adequate to characterize and analyze cell biological properties precisely and rapidly. Along with the processing speed of the microfluidic platform for the chosen approaches, one should take into account the following two time considerations: (i) Sample preparation time and (ii) data analysis. In reality, it is true that a fairly large amount of time is spent for sample preparation before microfluidic tests to deal with large and heterogeneous cell samples. In addition, we cannot ignore the time to analyze readouts from the microfluidic platforms to extract meaningful data as post processing. For example, an image stack from a high-speed camera should be processed, and electrical signals should be translated into useful cell biophysical properties later. Therefore, true high-speed cell manipulation processing can be attained considering all time requirements, and a holistic effort to reduce time for sample preparation, sample processing, and data analysis should be pursued simultaneously.

Acknowledgments

The authors would like to thank Kevin Paulsen and Michael Cintron for their useful comments.

References

1. Kovarik, M.L., Gach, P.C., Ornoff, D.M., Wang, Y., Balowski, J., Farrag, L., and Allbritton, N.L. (2011) Micro total analysis systems for cell biology and biochemical assays. *Anal. Chem.*, **84** (2), 516–540.
2. Haeberle, S. and Zengerle, R. (2007) Microfluidic platforms for lab-on-a-chip applications. *Lab Chip*, **7** (9), 1094–1110.
3. Takayama, S., Ostuni, E., LeDuc, P., Naruse, K., Ingber, D.E., and Whitesides, G.M. (2001) Subcellular positioning of small molecules. *Nature*, **411** (6841), 1016.
4. Takayama, S., Ostuni, E., LeDuc, P., Naruse, K., Ingber, D.E., and Whitesides, G.M. (2003) Selective chemical treatment of cellular microdomains using multiple laminar streams. *Chem. Biol.*, **10** (2), 123–130.
5. Weaver, W.M., Tseng, P., Kunze, A., Masaeli, M., Chung, A.J., Dudani, J.S., Kittur, H., Kulkarni, R.P., and Di Carlo, D. (2014) Advances in high-throughput single-cell microtechnologies. *Curr. Opin. Biotechnol.*, **25**, 114–123.
6. El-Ali, J., Sorger, P.K., and Jensen, K.F. (2006) Cells on chips. *Nature*, **442** (7101), 403–411.
7. Stone, H.A., Stroock, A.D., and Ajdari, A. (2004) Engineering flows in small devices: microfluidics toward a lab-on-a-chip. *Annu. Rev. Fluid Mech.*, **36** (1), 381–411.

8. Erickson, D. and Li, D. (2004) Integrated microfluidic devices. *Anal. Chim. Acta*, **507** (1), 11–26.
9. Melin, J. and Quake, S.R. (2007) Microfluidic large-scale integration: the evolution of design rules for biological automation. *Annu. Rev. Biophys. Biomol. Struct.*, **36** (1), 213–231.
10. Kim, S.M., Lee, S.H., and Suh, K.Y. (2008) Cell research with physically modified microfluidic channels: a review. *Lab Chip*, **8** (7), 1015–1023.
11. Mu, X., Zheng, W., Sun, J., Zhang, W., and Jiang, X. (2013) Microfluidics for manipulating cells. *Small*, **9** (1), 9–21.
12. Zheng, Y., Nguyen, J., Wei, Y., and Sun, Y. (2013) Recent advances in microfluidic techniques for single-cell biophysical characterization. *Lab Chip*, **13** (13), 2464–2483.
13. Yi, C., Li, C.-W., Ji, S., and Yang, M. (2006) Microfluidics technology for manipulation and analysis of biological cells. *Anal. Chim. Acta*, **560** (1), 1–23.
14. Andersson, H. and van den Berg, A. (2003) Microfluidic devices for cellomics: a review. *Sens. Actuators B*, **92** (3), 315–325.
15. Yun, H., Kim, K., and Lee, W.G. (2013) Cell manipulation in microfluidics. *Biofabrication*, **5** (2), 022001.
16. Jin, C., McFaul, S.M., Duffy, S.P., Deng, X., Tavassoli, P., Black, P.C., and Ma, H. (2014) Technologies for label-free separation of circulating tumor cells: from historical foundations to recent developments. *Lab Chip*, **14** (1), 32–44.
17. Hyun, K.-A. and Jung, H.-I. (2014) Advances and critical concerns with the microfluidic enrichments of circulating tumor cells. *Lab Chip*, **14** (1), 45–56.
18. Mach, A.J., Adeyiga, O.B., and Di Carlo, D. (2013) Microfluidic sample preparation for diagnostic cytopathology. *Lab Chip*, **13** (6), 1011–1026.
19. Young, E.W.K. and Beebe, D.J. (2010) Fundamentals of microfluidic cell culture in controlled microenvironments. *Chem. Soc. Rev.*, **39** (3), 1036–1048.
20. Carlo, D.D. and Lee, L.P. (2006) Dynamic single-cell analysis for quantitative biology. *Anal. Chem.*, **78** (23), 7918–7925.
21. Yung, C.W., Fiering, J., Mueller, A.J., and Ingber, D.E. (2009) Micromagnetic-microfluidic blood cleansing device. *Lab Chip*, **9** (9), 1171–1177.
22. Pantoja, R., Nagarah, J.M., Starace, D.M., Melosh, N.A., Blunck, R., Bezanilla, F., and Heath, J.R. (2004) Silicon chip-based patch-clamp electrodes integrated with PDMS microfluidics. *Biosens. Bioelectron.*, **20** (3), 509–517.
23. Jang, L.-S. and Wang, M.-H. (2007) Microfluidic device for cell capture and impedance measurement. *Biomed. Microdevices*, **9** (5), 737–743.
24. Malleo, D., Nevill, J.T., Lee, L.P., and Morgan, H. (2010) Continuous differential impedance spectroscopy of single cells. *Microfluid. Nanofluid.*, **9** (2-3), 191–198.
25. Yun, H. and Hur, S.C. (2013) Sequential multi-molecule delivery using vortex-assisted electroporation. *Lab Chip*, **13** (14), 2764–2772.
26. Bao, N., Kodippili, G.C., Giger, K.M., Fowler, V.M., Low, P.S., and Lu, C. (2011) Single-cell electrical lysis of erythrocytes detects deficiencies in the cytoskeletal protein network. *Lab Chip*, **11** (18), 3053–3056.
27. Sun, T. and Morgan, H. (2010) Single-cell microfluidic impedance cytometry: a review. *Microfluid. Nanofluid.*, **8** (4), 423–443.
28. Cheung, K.C., Di Berardino, M., Schade-Kampmann, G., Hebeisen, M., Pierzchalski, A., Bocsi, J., Mittag, A., and Tárnok, A. (2010) Microfluidic impedance-based flow cytometry. *Cytometry A*, **77A** (7), 648–666.
29. Heikali, D. and Di Carlo, D. (2010) A niche for microfluidics in portable hematology analyzers. *J. Assoc. Lab. Autom.*, **15** (4), 319–328.
30. Schade-Kampmann, G., Huwiler, A., Hebeisen, M., Hessler, T., and Di Berardino, M. (2008) On-chip non-invasive and label-free cell discrimination by impedance spectroscopy. *Cell Prolif.*, **41** (5), 830–840.
31. Holmes, D., Pettigrew, D., Reccius, C.H., Gwyer, J.D., van Berkel, C., Holloway, J., Davies, D.E., and Morgan, H. (2009) Leukocyte analysis and differentiation using high speed microfluidic

single cell impedance cytometry. *Lab Chip*, **9** (20), 2881–2889.
32. Pierzchalski, A., Hebeisen, M., Mittag, A., Di Berardino, M., and Tarnok, A. (2010) Label-free single cell analysis with a chip-based impedance flow cytometer. BiOS. 2010: International Society for Optics and Photonics.
33. Cheung, K., Gawad, S., and Renaud, P. (2005) Impedance spectroscopy flow cytometry: on-chip label-free cell differentiation. *Cytometry A*, **65A** (2), 124–132.
34. Du, E., Ha, S., Diez-Silva, M., Dao, M., Suresh, S., and Chandrakasan, A.P. (2013) Electric impedance microflow cytometry for characterization of cell disease states. *Lab Chip*, **13** (19), 3903–3909.
35. Haandbæk, N., Burgel, S.C., Heer, F., and Hierlemann, A. (2014) Characterization of subcellular morphology of single yeast cells using high frequency microfluidic impedance cytometer. *Lab Chip*, **14** (2), 369–377.
36. Pamme, N. (2006) Magnetism and microfluidics. *Lab Chip*, **6** (1), 24–38.
37. Gijs, M.A. (2004) Magnetic bead handling on-chip: new opportunities for analytical applications. *Microfluid. Nanofluid.*, **1** (1), 22–40.
38. Kilinc, D. and Lee, G.U. (2014) Advances in magnetic tweezers for single molecule and cell biophysics. *Integr. Biol.*, **6** (1), 27–34.
39. De Vlaminck, I. and Dekker, C. (2012) Recent advances in magnetic tweezers. *Annu. Rev. Biophys.*, **41** (1), 453–472.
40. Lautenschläger, F., Paschke, S., Schinkinger, S., Bruel, A., Beil, M., and Guck, J. (2009) The regulatory role of cell mechanics for migration of differentiating myeloid cells. *Proc. Natl. Acad. Sci. U.S.A.*, **106** (37), 15696–15701.
41. Lincoln, B., Erickson, H.M., Schinkinger, S., Wottawah, F., Mitchell, D., Ulvick, S., Bilby, C., and Guck, J. (2004) Deformability-based flow cytometry. *Cytometry A*, **59A** (2), 203–209.
42. Guck, J., Ananthakrishnan, R., Mahmood, H., Moon, T.J., Cunningham, C.C., and Käs, J. (2001) The optical stretcher: a novel laser tool to micromanipulate cells. *Biophys. J.*, **81** (2), 767–784.
43. Remmerbach, T.W., Wottawah, F., Dietrich, J., Lincoln, B., Wittekind, C., and Guck, J. (2009) Oral cancer diagnosis by mechanical phenotyping. *Cancer Res.*, **69** (5), 1728–1732.
44. Ashkin, A., Dziedzic, J., and Yamane, T. (1987) Optical trapping and manipulation of single cells using infrared laser beams. *Nature*, **330** (6150), 769–771.
45. Piggee, C. (2008) Optical tweezers: not just for physicists anymore. *Anal. Chem.*, **81** (1), 16–19.
46. Neuman, K.C. and Block, S.M. (2004) Optical trapping. *Rev. Sci. Instrum.*, **75** (9), 2787–2809.
47. Grier, D.G. (2003) A revolution in optical manipulation. *Nature*, **424** (6950), 810–816.
48. Zhang, H. and Liu, K.-K. (2008) Optical tweezers for single cells. *J. R. Soc. Interface*, **5** (24), 671–690.
49. Dholakia, K., Reece, P., and Gu, M. (2008) Optical micromanipulation. *Chem. Soc. Rev.*, **37** (1), 42–55.
50. Padgett, M. and Di Leonardo, R. (2011) Holographic optical tweezers and their relevance to lab on chip devices. *Lab Chip*, **11** (7), 1196–1205.
51. Di Carlo, D. (2012) A mechanical biomarker of cell state in medicine. *Jala*, **17** (1), 32–42.
52. Mao, X. and Huang, T.J. (2012) Exploiting mechanical biomarkers in microfluidics. *Lab Chip*, **12** (20), 4006–4009.
53. Zheng, Y., Shojaei-Baghini, E., Azad, A., Wang, C., and Sun, Y. (2012) High-throughput biophysical measurement of human red blood cells. *Lab Chip*, **12** (14), 2560–2567.
54. Adamo, A., Sharei, A., Adamo, L., Lee, B., Mao, S., and Jensen, K.F. (2012) Microfluidics-based assessment of cell deformability. *Anal. Chem.*, **84** (15), 6438–6443.
55. Byun, S., Son, S., Amodei, D., Cermak, N., Shaw, J., Kang, J.H., Hecht, V.C., Winslow, M.M., Jacks, T., Mallick, P., and Manalis, S.R. (2013) Characterizing deformability and surface friction

of cancer cells. *Proc. Natl. Acad. Sci. U.S.A.*, **110** (19), 7580–7585.
56. Zhang, W., Kai, K., Choi, D.S., Iwamoto, T., Nguyen, Y.H., Wong, H., Landis, M.D., Ueno, N.T., Chang, J., and Qin, L. (2012) Microfluidics separation reveals the stem-cell–like deformability of tumor-initiating cells. *Proc. Natl. Acad. Sci. U.S.A.*
57. Dudani, J.S., Gossett, D.R., Tse, H.T.K., and Di Carlo, D. (2013) Pinched-flow hydrodynamic stretching of single-cells. *Lab Chip*, **13** (18), 3728–3734.
58. Cha, S., Shin, T., Lee, S.S., Shim, W., Lee, G., Lee, S.J., Kim, Y., and Kim, J.M. (2012) Cell stretching measurement utilizing viscoelastic particle focusing. *Anal. Chem.*, **84** (23), 10471–10477.
59. Huang, S., Undisz, A., Diez-Silva, M., Bow, H., Dao, M., and Han, J. (2013) Dynamic deformability of Plasmodium falciparum-infected erythrocytes exposed to artesunate in vitro. *Integr. Biol.*, **5** (2), 414–422.
60. Huang, S., Amaladoss, A., Liu, M., Chen, H., Zhang, R., Preiser, P.R., Dao, M., and Han, J. (2014) In vivo splenic clearance correlates with in vitro deformability of red blood cells from plasmodium yoelii-infected mice. *Infect. Immun.*, **82** (6), 2532–2541.
61. Burg, T.P., Godin, M., Knudsen, S.M., Shen, W., Carlson, G., Foster, J.S., Babcock, K., and Manalis, S.R. (2007) Weighing of biomolecules, single cells and single nanoparticles in fluid. *Nature*, **446** (7139), 1066–1069.
62. Preira, P., Grandne, V., Forel, J.M., Gabriele, S., Camara, M., and Theodoly, O. (2013) Passive circulating cell sorting by deformability using a microfluidic gradual filter. *Lab Chip*, **13** (1), 161–170.
63. Beattie, W., Qin, X., Wang, L., and Ma, H. (2014) Clog-free cell filtration using resettable cell traps. *Lab Chip*, **14** (15), 2657–2665.
64. Toner, M. and Irimia, D. (2005) Blood-on-a-chip. *Ann. Rev. Biomed. Eng.*, **7** (1), 77–103.
65. Lee, S., Yim, Y., Ahn, K., and Lee, S. (2009) Extensional flow-based assessment of red blood cell deformability using hyperbolic converging microchannel. *Biomed. Microdevices*, **11** (5), 1021–1027.
66. Forsyth, A.M., Wan, J., Ristenpart, W.D., and Stone, H.A. (2010) The dynamic behavior of chemically "stiffened" red blood cells in microchannel flows. *Microvasc. Res.*, **80** (1), 37–43.
67. Forsyth, A.M., Wan, J., Owrutsky, P.D., Abkarian, M., and Stone, H.A. (2011) Multiscale approach to link red blood cell dynamics, shear viscosity, and ATP release. *Proc. Natl. Acad. Sci. U.S.A.*, **108** (27), 10986–10991.
68. Park, H.Y., Qiu, X.Y., Rhoades, E., Korlach, J., Kwok, L.W., Zipfel, W.R., Webb, W.W., and Pollack, L. (2006) Achieving uniform mixing in a microfluidic device: hydrodynamic focusing prior to mixing. *Anal. Chem.*, **78** (13), 4465–4473.
69. Lee, G.-B., Chang, C.-C., Huang, S.-B., and Yang, R.-J. (2006) The hydrodynamic focusing effect inside rectangular microchannels. *J. Micromech. Microeng.*, **16** (5), 1024.
70. Amini, H., Lee, W., and Di Carlo, D. (2014) Inertial microfluidic physics. *Lab Chip*, **14** (15), 2739–2761.
71. Di Carlo, D. (2009) Inertial microfluidics. *Lab Chip*, **9** (21), 3038–3046.
72. Martel, J.M. and Toner, M. (2014) Inertial focusing in microfluidics. *Annu. Rev. Biomed. Eng.*, **16** (1), 371–396.
73. Gossett, D.R., Tse, H.T.K., Lee, S.A., Ying, Y., Lindgren, A.G., Yang, O.O., Rao, J., Clark, A.T., and Di Carlo, D. (2012) Hydrodynamic stretching of single cells for large population mechanical phenotyping. *Proc. Natl. Acad. Sci. U.S.A.*, **109** (20), 7630–7635.
74. Tse, H.T.K., Gossett, D.R., Moon, Y.S., Masaeli, M., Sohsman, M., Ying, Y., Mislick, K., Adams, R.P., Rao, J., and Di Carlo, D. (2013) Quantitative diagnosis of malignant pleural effusions by single-cell mechanophenotyping. *Sci. Transl. Med.*, **5** (212), 212ra163.
75. Yang, S., Kim, J.Y., Lee, S.J., Lee, S.S., and Kim, J.M. (2011) Sheathless elasto-inertial particle focusing and continuous separation in a straight rectangular microchannel. *Lab Chip*, **11** (2), 266–273.

76. Nam, J., Lim, H., Kim, D., Jung, H., and Shin, S. (2012) Continuous separation of microparticles in a microfluidic channel via the elasto-inertial effect of non-Newtonian fluid. *Lab Chip*, **12** (7), 1347–1354.
77. Goda, K., Tsia, K., and Jalali, B. (2009) Serial time-encoded amplified imaging for real-time observation of fast dynamic phenomena. *Nature*, **458** (7242), 1145–1149.
78. Goda, K., Ayazi, A., Gossett, D.R., Sadasivam, J., Lonappan, C.K., Sollier, E., Fard, A.M., Hur, S.C., Adam, J., Murray, C., Wang, C., Brackbill, N., Di Carlo, D., and Jalali, B. (2012) High-throughput single-microparticle imaging flow analyzer. *Proc. Natl. Acad. Sci. U.S.A.*, **109** (29), 11630–11635.
79. Tse, H.T.K., Meng, P., Gossett, D.R., Irturk, A., Kastner, R., and Di Carlo, D. (2011) Strategies for implementing hardware-assisted high-throughput cellular image analysis. *J. Assoc. Lab. Automat.*, **16** (6), 422–430.
80. Gao, Y., Li, W., and Pappas, D. (2013) Recent advances in microfluidic cell separations. *Analyst*, **138** (17), 4714–4721.
81. Gossett, D.R., Weaver, W.M., Mach, A.J., Hur, S.C., Tse, H.T.K., Lee, W., Amini, H., and Di Carlo, D. (2010) Label-free cell separation and sorting in microfluidic systems. *Anal. Bioanal.Chem.*, **397** (8), 3249–3267.
82. Jackson, E.L. and Lu, H. (2013) Advances in microfluidic cell separation and manipulation. *Curr. Opin. Chem. Eng.*, **2** (4), 398–404.
83. Geislinger, T.M. and Franke, T. (2014) Hydrodynamic lift of vesicles and red blood cells in flow—from Fåhræus & Lindqvist to microfluidic cell sorting. *Adv. Colloid Interface Sci.*, **208**, 161–176.
84. Bhagat, A.A.S., Bow, H., Hou, H.W., Tan, S.J., Han, J., and Lim, C.T. (2010) Microfluidics for cell separation. *Med. Biol. Eng. Comput.*, **48** (10), 999–1014.
85. Hou, H.W., Lee, W.C., Leong, M.C., Sonam, S., Vedula, S.R.K., and Lim, C.T. (2011) Microfluidics for applications in cell mechanics and mechanobiology. *Cell. Mol. Bioeng.*, **4** (4), 591–602.
86. Çetin, B., Özer, M.B., and Solmaz, M.E. (2014) Microfluidic bio-particle manipulation for biotechnology. *Biochem. Eng. J.*
87. Pratt, E.D., Huang, C., Hawkins, B.G., Gleghorn, J.P., and Kirby, B.J. (2011) Rare cell capture in microfluidic devices. *Chem. Eng. Sci.*, **66** (7), 1508–1522.
88. Faivre, M., Abkarian, M., Bickraj, K., and Stone, H.A. (2006) Geometrical focusing of cells in a microfluidic device: an approach to separate blood plasma. *Biorheology*, **43** (2), 147–159.
89. Warkiani, M.E., Guan, G., Luan, K.B., Lee, W.C., Bhagat, A.A.S., Kant Chaudhuri, P., Tan, D.S.-W., Lim, W.T., Lee, S.C., Chen, P.C.Y., Lim, C.T., and Han, J. (2014) Slanted spiral microfluidics for the ultra-fast, label-free isolation of circulating tumor cells. *Lab Chip*, **14** (1), 128–137.
90. Warkiani, M.E., Khoo, B.L., Tan, D.S.-W., Bhagat, A.A.S., Lim, W.-T., Yap, Y.S., Lee, S.C., Soo, R.A., Han, J., and Lim, C.T. (2014) An ultra-high-throughput spiral microfluidic biochip for the enrichment of circulating tumor cells. *Analyst*, **139** (13), 3245–3255.
91. Lee, M.G., Shin, J.H., Bae, C.Y., Choi, S., and Park, J.-K. (2013) Label-free cancer cell separation from human whole blood using inertial microfluidics at low shear stress. *Anal. Chem.*, **85** (13), 6213–6218.
92. Inglis, D.W., Lord, M., and Nordon, R.E. (2011) Scaling deterministic lateral displacement arrays for high throughput and dilution-free enrichment of leukocytes. *J. Micromech. Microeng.*, **21** (5), 054024.
93. Holm, S.H., Beech, J.P., Barrett, M.P., and Tegenfeldt, J.O. (2011) Separation of parasites from human blood using deterministic lateral displacement. *Lab Chip*, **11** (7), 1326–1332.
94. Hou, H.W., Warkiani, M.E., Khoo, B.L., Li, Z.R., Soo, R.A., Tan, D.S.-W., Lim, W.-T., Han, J., Bhagat, A.A.S., and Lim, C.T. (2013) Isolation and retrieval of circulating tumor cells using centrifugal forces. *Sci. Rep.*, **3**, 1259.

95. Hou, H.W., Bhagat, A.A.S., Chong, A.G.L., Mao, P., Tan, K.S.W., Han, J., and Lim, C.T. (2010) Deformability based cell margination—a simple microfluidic design for malaria-infected erythrocyte separation. *Lab Chip*, **10** (19), 2605–2613.
96. Huang, L.R., Cox, E.C., Austin, R.H., and Sturm, J.C. (2004) Continuous particle separation through deterministic lateral displacement. *Science*, **304** (5673), 987–990.
97. McGrath, J.S., Jimenez, M., and Bridle, H.L. (2014) Deterministic lateral displacement for particle separation: a review. *Lab Chip*, **14** (21), 4139–4158.
98. Inglis, D.W., Davis, J.A., Austin, R.H., and Sturm, J.C. (2006) Critical particle size for fractionation by deterministic lateral displacement. *Lab Chip*, **6** (5), 655–658.
99. Loutherback, K., D'Silva, J., Liu, L., Wu, A., Austin, R.H., and Sturm, J.C. (2012) Deterministic separation of cancer cells from blood at 10 mL/min. *AIP Adv.*, **2** (4), 042107.
100. Mach, A.J. and Di Carlo, D. (2010) Continuous scalable blood filtration device using inertial microfluidics. *Biotechnol. Bioeng.*, **107** (2), 302–311.
101. Liu, Z., Huang, F., Du, J., Shu, W., Feng, H., Xu, X., and Chen, Y. (2013) Rapid isolation of cancer cells using microfluidic deterministic lateral displacement structure. *Biomicrofluidics*, **7** (1), 011801.
102. Ho, B.P. and Leal, L.G. (1974) Inertial migration of rigid spheres in two-dimensional unidirectional flows. *J. Fluid Mech.*, **65** (02), 365–400.
103. Zhou, J., Giridhar, P.V., Kasper, S., and Papautsky, I. (2013) Modulation of aspect ratio for complete separation in an inertial microfluidic channel. *Lab Chip*, **13** (10), 1919–1929.
104. Shen, S., Ma, C., Zhao, L., Wang, Y., Wang, J.-C., Xu, J., Li, T., Pang, L., and Wang, J. (2014) High-throughput rare cell separation from blood samples using steric hindrance and inertial microfluidics. *Lab Chip*, **14**, 2525–2538.
105. Bhagat, A.A.S., Hou, H.W., Li, L.D., Lim, C.T., and Han, J. (2011) Pinched flow coupled shear-modulated inertial microfluidics for high-throughput rare blood cell separation. *Lab Chip*, **11** (11), 1870–1878.
106. Moon, H.-S., Kwon, K., Hyun, K.-A., Sim, T.S., Park, J.C., Lee, J.-G., and Jung, H.-I. (2013) Continual collection and re-separation of circulating tumor cells from blood using multi-stage multi-orifice flow fractionation. *Biomicrofluidics*, **7** (1), 014105.
107. Hur, S.C., Mach, A.J., and Di Carlo, D. (2011) High-throughput size-based rare cell enrichment using microscale vortices. *Biomicrofluidics*, **5** (2), 022206.
108. Mach, A.J., Kim, J.H., Arshi, A., Hur, S.C., and Di Carlo, D. (2011) Automated cellular sample preparation using a Centrifuge-on-a-Chip. *Lab Chip*, **11** (17), 2827–2834.
109. Che, J., Mach, A.J., Go, D.E., Talati, I., Ying, Y., Rao, J.Y., Kulkarni, R.P., and Di Carlo, D. (2013) Microfluidic purification and concentration of malignant pleural effusions for improved molecular and cytomorphological diagnostics. *PLoS One*, **8** (10), e78194.
110. Sollier, E., Go, D.E., Che, J., Gossett, D.R., O'Byrne, S., Weaver, W.M., Kummer, N., Rettig, M., Goldman, J., and Nickols, N. (2014) Size-selective collection of circulating tumor cells using vortex technology. *Lab Chip*, **14** (1), 63–77.
111. Berger, S.A., Talbot, L., and Yao, L.S. (1983) Flow in curved pipes. *Annu. Rev. Fluid Mech.*, **15**, 461–512.
112. Di Carlo, D., Edd, J.F., Irimia, D., Tompkins, R.G., and Toner, M. (2008) Equilibrium separation and filtration of particles using differential inertial focusing. *Anal. Chem.*, **80** (6), 2204–2211.
113. Zhang, J., Yan, S., Sluyter, R., Li, W., Alici, G., and Nguyen, N.-T. (2014) Inertial particle separation by differential equilibrium positions in a symmetrical serpentine micro-channel. *Sci. Rep.*, **4**.
114. Tanaka, T., Ishikawa, T., Numayama-Tsuruta, K., Imai, Y., Ueno, H., Matsuki, N., and Yamaguchi, T. (2012) Separation of cancer cells from a

red blood cell suspension using inertial force. *Lab Chip*, **12** (21), 4336–4343.

115. Nivedita, N. and Papautsky, I. (2013) Continuous separation of blood cells in spiral microfluidic devices. *Biomicrofluidics*, **7** (5), 054101.

116. Kuntaegowdanahalli, S.S., Bhagat, A.A.S., Kumar, G., and Papautsky, I. (2009) Inertial microfluidics for continuous particle separation in spiral microchannels. *Lab Chip*, **9** (20), 2973–2980.

117. Lee, W.C., Bhagat, A.A.S., Huang, S., Van Vliet, K.J., Han, J., and Lim, C.T. (2011) High-throughput cell cycle synchronization using inertial forces in spiral microchannels. *Lab Chip*, **11** (7), 1359–1367.

118. Khoo, B.L., Warkiani, M.E., Tan, D.S.-W., Bhagat, A.A.S., Irwin, D., Lau, D.P., Lim, A.S., Lim, K.H., Krisna, S.S., and Lim, W.-T. (2014) Clinical validation of an ultra high-throughput spiral microfluidics for the detection and enrichment of viable circulating tumor cells. *PLoS One*, **9** (7), e99409.

119. Sun, J., Li, M., Liu, C., Zhang, Y., Liu, D., Liu, W., Hu, G., and Jiang, X. (2012) Double spiral microchannel for label-free tumor cell separation and enrichment. *Lab Chip*, **12** (20), 3952–3960.

120. Guan, G., Wu, L., Bhagat, A.A., Li, Z., Chen, P.C., Chao, S., Ong, C.J., and Han, J. (2013) Spiral microchannel with rectangular and trapezoidal cross-sections for size based particle separation. *Sci. Rep.*, **3**.

121. Wu, L.D., Guan, G.F., Hou, H.W., Bhagat, A.A.S., and Han, J. (2012) Separation of leukocytes from blood using spiral channel with trapezoid cross-section. *Anal. Chem.*, **84** (21), 9324–9331.

122. Lee, W., Amini, H., Stone, H.A., and Di Carlo, D. (2010) Dynamic self-assembly and control of microfluidic particle crystals. *Proc. Natl. Acad. Sci. U.S.A.*, **107** (52), 22413–22418.

123. Fahraus, R. and Lindqvist, T. (1931) The viscosity of the blood in narrow capillary tubes. *Am. J. Physiol.*, **96** (3), 562–568.

124. Hur, S.C., Henderson-MacLennan, N.K., McCabe, E.R., and Di Carlo, D. (2011) Deformability-based cell classification and enrichment using inertial microfluidics. *Lab Chip*, **11** (5), 912–920.

125. Sugaya, S., Yamada, M., and Seki, M. (2011) Observation of nonspherical particle behaviors for continuous shape-based separation using hydrodynamic filtration. *Biomicrofluidics*, **5** (2), 024103.

126. Ozkumur, E., Shah, A.M., Ciciliano, J.C., Emmink, B.L., Miyamoto, D.T., Brachtel, E., Yu, M., Chen, P.-i., Morgan, B., and Trautwein, J. (2013) Inertial focusing for tumor antigen–dependent and–independent sorting of rare circulating tumor cells. *Sci. Transl. Med.*, **5** (179), 179ra147.

127. Sollier, E., Rostaing, H., Pouteau, P., Fouillet, Y., and Achard, J.-L. (2009) Passive microfluidic devices for plasma extraction from whole human blood. *Sens. Actuators B*, **141** (2), 617–624.

128. Jain, A. and Munn, L.L. (2009) Determinants of leukocyte margination in rectangular microchannels. *PLoS One*, **4** (9), e7104.

129. Magnaudet, J., Takagi, S., and Legendre, D. (2003) Drag, deformation and lateral migration of a buoyant drop moving near a wall. *J. Fluid Mech.*, **476**, 115–157.

130. Geislinger, T.M. and Franke, T. (2013) Sorting of circulating tumor cells (MV3-melanoma) and red blood cells using non-inertial lift. *Biomicrofluidics*, **7** (4), 044120.

131. Beech, J.P., Holm, S.H., Adolfsson, K., and Tegenfeldt, J.O. (2012) Sorting cells by size, shape and deformability. *Lab Chip*, **12** (6), 1048–1051.

132. Hur, S.C., Choi, S.-E., Kwon, S., and Di Carlo, D. (2011) Inertial focusing of non-spherical microparticles. *Appl. Phys. Lett.*, **99** (4), 044101.

133. Masaeli, M., Sollier, E., Amini, H., Mao, W., Camacho, K., Doshi, N., Mitragotri, S., Alexeev, A., and Di Carlo, D. (2012) Continuous inertial focusing and separation of particles by shape. *Phys. Rev. X*, **2** (3), 031017.

134. Hur, S.C., Brinckerhoff, T.Z., Walthers, C.M., Dunn, J.C., and Di Carlo, D. (2012) Label-free enrichment of adrenal cortical progenitor cells using inertial microfluidics. *PLoS One*, **7** (10), e46550.
135. Sajeesh, P. and Sen, A. (2014) Particle separation and sorting in microfluidic devices: a review. *Microfluid. Nanofluid.*, **17** (1), 1–52.
136. Watarai, H. (2013) Continuous separation principles using external microaction forces. *Annu. Rev. Anal. Chem.*, **6** (1), 353–378.
137. Lenshof, A. and Laurell, T. (2010) Continuous separation of cells and particles in microfluidic systems. *Chem. Soc. Rev.*, **39** (3), 1203–1217.
138. Yeo, L.Y. and Friend, J.R. (2014) Surface acoustic wave microfluidics. *Annu. Rev. Fluid Mech.*, **46** (1), 379–406.
139. Laurell, T., Petersson, F., and Nilsson, A. (2007) Chip integrated strategies for acoustic separation and manipulation of cells and particles. *Chem. Soc. Rev.*, **36** (3), 492–506.
140. Lenshof, A., Magnusson, C., and Laurell, T. (2012) Acoustofluidics 8: Applications of acoustophoresis in continuous flow microsystems. *Lab Chip*, **12** (7), 1210–1223.
141. Ding, X., Lin, S.-C.S., Kiraly, B., Yue, H., Li, S., Chiang, I.-K., Shi, J., Benkovic, S.J., and Huang, T.J. (2012) On-chip manipulation of single microparticles, cells, and organisms using surface acoustic waves. *Proc. Natl. Acad. Sci. U.S.A.*, **109** (28), 11105–11109.
142. Nam, J., Lim, H., Kim, D., and Shin, S. (2011) Separation of platelets from whole blood using standing surface acoustic waves in a microchannel. *Lab Chip*, **11** (19), 3361–3364.
143. Petersson, F., Åberg, L., Swärd-Nilsson, A.-M., and Laurell, T. (2007) Free flow acoustophoresis: microfluidic-based mode of particle and cell separation. *Anal. Chem.*, **79** (14), 5117–5123.
144. Yang, A.H.J. and Soh, H.T. (2012) Acoustophoretic sorting of viable mammalian cells in a microfluidic device. *Anal. Chem.*, **84** (24), 10756–10762.
145. Adams, J.D., Ebbesen, C.L., Barnkob, R., Yang, A.H.J., Soh, H.T., and Bruus, H. (2012) High-throughput, temperature-controlled microchannel acoustophoresis device made with rapid prototyping. *J. Micromech. Microeng.*, **22** (7), 075017.
146. Shim, S., Stemke-Hale, K., Tsimberidou, A.M., Noshari, J., Anderson, T.E., and Gascoyne, P.R. (2013) Antibody-independent isolation of circulating tumor cells by continuous-flow dielectrophoresis. *Biomicrofluidics*, **7** (1), 011807.
147. Adams, J.D., Kim, U., and Soh, H.T. (2008) Multitarget magnetic activated cell sorter. *Proc. Natl. Acad. Sci. U.S.A.*, **105** (47), 18165–18170.
148. Chen, Y., Chung, A.J., Wu, T.H., Teitell, M.A., Di Carlo, D., and Chiou, P.Y. (2014) Pulsed laser activated cell sorting with three dimensional sheathless inertial focusing. *Small*, **10** (9), 1746–1751.
149. Kirby, B.J. (2010) *Micro-and Nanoscale Fluid Mechanics: Transport in Microfluidic Devices*, Cambridge University Press.
150. Pethig, R. (2010) Review Article—Dielectrophoresis: Status of the theory, technology, and applications. *Biomicrofluidics*, **4** (2), 022811.
151. Kang, Y., Li, D., Kalams, S.A., and Eid, J.E. (2008) DC-Dielectrophoretic separation of biological cells by size. *Biomed. Microdevices*, **10** (2), 243–249.
152. Yang, J., Huang, Y., Wang, X.-B., Becker, F.F., and Gascoyne, P.R.C. (2000) Differential analysis of human leukocytes by dielectrophoretic field-flow-fractionation. *Biophys. J.*, **78** (5), 2680–2689.
153. Gascoyne, P.R.C., Noshari, J., Anderson, T.J., and Becker, F.F. (2009) Isolation of rare cells from cell mixtures by dielectrophoresis. *Electrophoresis*, **30** (8), 1388–1398.
154. Piacentini, N., Mernier, G., Tornay, R., and Renaud, P. (2011) Separation of platelets from other blood cells in continuous-flow by dielectrophoresis field-flow-fractionation. *Biomicrofluidics*, **5** (3), 34122–341228.

155. Kim, U., Shu, C.-W., Dane, K.Y., Daugherty, P.S., Wang, J.Y., and Soh, H. (2007) Selection of mammalian cells based on their cell-cycle phase using dielectrophoresis. *Proc. Natl. Acad. Sci. U.S.A.*, **104** (52), 20708–20712.
156. Alazzam, A., Stiharu, I., Bhat, R., and Meguerditchian, A.-N. (2011) Interdigitated comb-like electrodes for continuous separation of malignant cells from blood using dielectrophoresis. *Electrophoresis*, **32** (11), 1327–1336.
157. Park, S., Zhang, Y., Wang, T.-H., and Yang, S. (2011) Continuous dielectrophoretic bacterial separation and concentration from physiological media of high conductivity. *Lab Chip*, **11** (17), 2893–2900.
158. Melville, D., Paul, F., and Roath, S. (1975) Direct magnetic separation of red cells from whole blood. *Nature*, **255** (5511), 706–706.
159. Miltenyi, S., Muller, W., Weichel, W., and Radbruch, A. (1990) High gradient magnetic cell separation with MACS. *Cytometry*, **11** (2), 231–238.
160. Iversen, T.-G., Skotland, T., and Sandvig, K. (2011) Endocytosis and intracellular transport of nanoparticles: Present knowledge and need for future studies. *Nano Today*, **6** (2), 176–185.
161. Robert, D., Pamme, N., Conjeaud, H., Gazeau, F., Iles, A., and Wilhelm, C. (2011) Cell sorting by endocytotic capacity in a microfluidic magnetophoresis device. *Lab Chip*, **11** (11), 1902–1910.
162. Jones, C.F. and Grainger, D.W. (2009) In vitro assessments of nanomaterial toxicity. *Adv. Drug Delivery Rev.*, **61** (6), 438–456.
163. Tseng, P., Judy, J.W., and Di Carlo, D. (2012) Magnetic nanoparticle-mediated massively parallel mechanical modulation of single-cell behavior. *Nat. Methods*, **9** (11), 1113–1119.
164. MacDonald, M., Spalding, G., and Dholakia, K. (2003) Microfluidic sorting in an optical lattice. *Nature*, **426** (6965), 421–424.
165. Baumgartl, J., Hannappel, G.M., Stevenson, D.J., Day, D., Gu, M., and Dholakia, K. (2009) Optical redistribution of microparticles and cells between microwells. *Lab Chip*, **9** (10), 1334–1336.
166. Wang, M.M., Tu, E., Raymond, D.E., Yang, J.M., Zhang, H.C., Hagen, N., Dees, B., Mercer, E.M., Forster, A.H., Kariv, I., Marchand, P.J., and Butler, W.F. (2005) Microfluidic sorting of mammalian cells by optical force switching. *Nat. Biotechnol.*, **23** (1), 83–87.
167. Piyasena, M.E. and Graves, S.W. (2014) The intersection of flow cytometry with microfluidics and microfabrication. *Lab Chip*, **14** (6), 1044–1059.
168. Karabacak, N.M., Spuhler, P.S., Fachin, F., Lim, E.J., Pai, V., Ozkumur, E., Martel, J.M., Kojic, N., Smith, K., and Chen, P.-I. (2014) Microfluidic, marker-free isolation of circulating tumor cells from blood samples. *Nat. Protoc.*, **9** (3), 694–710.
169. Mizuno, M., Yamada, M., Mitamura, R., Ike, K., Toyama, K., and Seki, M. (2013) Magnetophoresis-integrated hydrodynamic filtration system for size-and surface marker-based two-dimensional cell sorting. *Anal. Chem.*, **85** (16), 7666–7673.
170. Parichehreh, V., Medepallai, K., Babbarwal, K., and Sethu, P. (2013) Microfluidic inertia enhanced phase partitioning for enriching nucleated cell populations in blood. *Lab Chip*, **13** (5), 892–900.
171. Seo, H.-K., Kim, Y.-H., Kim, H.-O., and Kim, Y.-J. (2010) Hybrid cell sorters for on-chip cell separation by hydrodynamics and magnetophoresis. *J. Micromech. Microeng.*, **20** (9), 095019.
172. Choi, S., Levy, O., Coelho, M.B., Cabral, J.M., Karp, J.M., and Karnik, R. (2014) A cell rolling cytometer reveals the correlation between mesenchymal stem cell dynamic adhesion and differentiation state. *Lab Chip*, **14** (1), 161–166.
173. Xuan, X.C., Zhu, J.J., and Church, C. (2010) Particle focusing in microfluidic devices. *Microfluid. Nanofluid.*, **9** (1), 1–16.
174. Martel, J.M. and Toner, M. (2012) Inertial focusing dynamics in spiral microchannels. *Phys. Fluids*, **24** (3), 032001.

175. Martel, J.M. and Toner, M. (2013) Particle focusing in curved microfluidic channels. *Sci. Rep.*, **3** (3340), 1–8.

176. Oakey, J., Applegate, R.W., Arellano, E., Di Carlo, D., Graves, S.W., and Toner, M. (2010) Particle focusing in staged inertial microfluidic devices for flow cytometry. *Anal. Chem.*, **82** (9), 3862–3867.

177. Bhagat, A.A.S., Kuntaegowdanahalli, S.S., Kaval, N., Seliskar, C.J., and Papautsky, I. (2010) Inertial microfluidics for sheath-less high-throughput flow cytometry. *Biomed. Microdevices*, **12** (2), 187–195.

178. Chung, A.J., Gossett, D.R., and Di Carlo, D. (2013) Three dimensional, sheathless, and high-throughput microparticle inertial focusing through geometry-induced secondary flows. *Small*, **9** (5), 685–690.

179. Chung, A.J., Pulido, D., Oka, J.C., Amini, H., Masaeli, M., and Di Carlo, D. (2013) Microstructure-induced helical vortices allow single-stream and long-term inertial focusing. *Lab Chip*, **13** (15), 2942–2949.

180. Hur, S.C., Tse, H.T.K., and Di Carlo, D. (2010) Sheathless inertial cell ordering for extreme throughput flow cytometry. *Lab Chip*, **10** (3), 274–280.

181. Chen, Y., Nawaz, A.A., Zhao, Y., Huang, P.-H., McCoy, J.P., Levine, S.J., Wang, L., and Huang, T.J. (2014) Standing surface acoustic wave (SSAW)-based microfluidic cytometer. *Lab Chip*, **14** (5), 916–923.

182. Shi, J., Yazdi, S., Steven Lin, S.-C., Ding, X., Chiang, I.K., Sharp, K., and Huang, T.J. (2011) Three-dimensional continuous particle focusing in a microfluidic channel via standing surface acoustic waves (SSAW). *Lab Chip*, **11** (14), 2319–2324.

183. Shi, J., Huang, H., Stratton, Z., Huang, Y., and Huang, T.J. (2009) Continuous particle separation in a microfluidic channel via standing surface acoustic waves (SSAW). *Lab Chip*, **9** (23), 3354–3359.

184. Jakobsson, O., Grenvall, C., Nordin, M., Evander, M., and Laurell, T. (2014) Acoustic actuated fluorescence activated sorting of microparticles. *Lab Chip*, **14** (11), 1943–1950.

185. Zucker, R.M. and Fisher, N.C.,. (2001) *Evaluation and Purchase of an Analytical Flow Cytometer: Some of the Numerous Factors to Consider*, Current Protocols in Cytometry, John Wiley & Sons, Inc., New York.

186. Duda, D.G., Cohen, K.S., Scadden, D.T., and Jain, R.K. (2007) A protocol for phenotypic detection and enumeration of circulating endothelial cells and circulating progenitor cells in human blood. *Nat. Protoc.*, **2** (4), 805–810.

187. Gossett, D.R., Tse, H.T.K., Dudani, J.S., Goda, K., Woods, T.A., Graves, S.W., and Di Carlo, D. (2012) Inertial manipulation and transfer of microparticles across laminar fluid streams. *Small*, **8** (17), 2757–2764.

188. Tan, A.P., Dudani, J.S., Arshi, A., Lee, R.J., Tse, H.T.K., Gossett, D.R., and Di Carlo, D. (2014) Continuous-flow cytomorphological staining and analysis. *Lab Chip*, **14** (3), 522–531.

189. Dudani, J.S., Go, D.E., Gossett, D.R., Tan, A.P., and Di Carlo, D. (2014) Mediating millisecond reaction time around particles and cells. *Anal. Chem.*, **86** (3), 1502–1510.